

RS-8232-2/68625

SANDIA REPORT

SAND89-8465
Unlimited Release
Printed April 1989

cyz

Hydrodynamic Stability of Solid and Liquid Propellant Combustion



8232-2/068625



0000002 -

J. K. Bechtold and S. B. Margolis

Prepared by
Sandia National Laboratories
Albuquerque, New Mexico 87185 Livermore, California 94550
for the United States Department of Energy
under Contract DE-AC04-76DP00789

Issued by Sandia National Laboratories, operated for the United States Department of Energy by Sandia Corporation.

NOTICE: This report was prepared as an account of work sponsored by an agency of the United States Government. Neither the United States Government nor any agency thereof, nor any of their employees, nor any of the contractors, subcontractors, or their employees, makes any warranty, express or implied, or assumes any legal liability or responsibility for the accuracy, completeness, or usefulness of any information, apparatus, product, or process disclosed, or represents that its use would not infringe privately owned rights. Reference herein to any specific commercial product, process, or service by trade name, trademark, manufacturer, or otherwise, does not necessarily constitute or imply its endorsement, recommendation, or favoring by the United States Government, any agency thereof or any of their contractors or subcontractors. The views and opinions expressed herein do not necessarily state or reflect those of the United States Government, any agency thereof or any of their contractors or subcontractors.

SAND89-8465
Unlimited Release
Printed April 1989

HYDRODYNAMIC STABILITY OF SOLID AND LIQUID PROPELLANT COMBUSTION*

John K. Bechtold[†] and Stephen B. Margolis
Combustion Research Facility
Sandia National Laboratories, Livermore, California 94551

ABSTRACT

We derive a model which describes the dynamics of a multiphase system consisting of a gas flame attached to a pyrolyzing solid or liquid propellant. We consider the case in which the multiphase flame, which includes the propellant interface, the preheat zone and the gas-phase reaction zone, is thin compared to some characteristic hydrodynamic length. An asymptotic analysis of the inner structure then yields jump conditions on the fluid and transport variables across the multiphase flame, which is treated as a surface of discontinuity separating the unburned condensed-phase propellant from the burned gas. The resulting model, which describes the evolution of this surface, is then used to investigate the hydrodynamic (Landau) stability of propellant deflagration. In particular, it is shown that this type of instability is completely suppressed for solid propellants, whereas for liquid propellants, a cellular instability arises which is similar to that which occurs in premixed flame propagation.

*This work was supported by the Applied Mathematical Sciences Research Program, Office of Energy Research, U. S. Department of Energy.

[†]Sandia Postdoctoral Appointee

HYDRODYNAMIC STABILITY OF SOLID AND LIQUID PROPELLANT COMBUSTION

§1. Introduction

The phenomenon of hydrodynamic instability in premixed combustion theory was first described by Landau (1944) and Darrieus (1945) for the case of a freely propagating gas flame, and by Landau (1944) for the case of a liquid propellant. In both cases, it was assumed that the reaction front, corresponding to the flame and the liquid/gas interface, respectively, was infinitely thin and propagated normal to itself with a prescribed constant velocity. Due to the density jump across the front, the fluid variables are also discontinuous there, and a stability analysis of the gas flame leads to the prediction that plane flames are absolutely unstable to steady, but nonplanar (cellular), disturbances. A similar prediction was also made for the case of liquid propellants, although it was shown that the combined effects of gravity and surface tension were capable of stabilizing the reaction front in that problem.

Since plane flames are observable in the laboratory, it was clear that this simple phenomenological description of the reaction front as a hydrodynamic discontinuity was insufficient to completely characterize the nature of flame stability. Accordingly, this model of the gas flame was extended by Markstein (1951, 1964), who assumed a stabilizing phenomenological dependence of the propagation velocity on the curvature of the front. Further studies (*cf.* Einbinder, 1953; Eckhaus, 1961; Chu and Parlange, 1962; Istratov and Librovich, 1966) accounted for the finite thickness of the flame to obtain, from a perturbation analysis, corrections due to diffusional transport effects. Still more recent analyses of hydrodynamic instability in flames have sought to completely avoid any heuristic or phenomenological assumptions and to treat the the dynamic interaction of the flame with the underlying flow field. These studies (*cf.* Sivashinsky, 1977; Pelcé and Clavin, 1982; Frankel and Sivashinsky, 1982; Matalon and Matkowsky, 1982, 1983, 1984) treat the flame as an internal boundary layer on a hydrodynamical length scale, where the boundary layer is composed of a pre-heat zone and an even thinner reactive/diffusive zone. Formal asymptotic matching techniques are then used to derive jump conditions on the fluid variables across the flame structure. This type of analysis is consistent with the original notion of a flame as a hydrodynamic discontinuity, but does not require any *a priori* assumptions on the propagation velocity. For freely-propagating flames, it has been possible to obtain, for long-wave disturbances, an expression for the growth rate in the form of a power series expansion in the disturbance wavenumber. The first term in this expansion gives the classical result due to Landau (1944) and Darrieus (1945) that the growth rate is proportional to the wavenumber of the disturbance. However, the next term in this expansion can be stabilizing, suggesting that this type of hydrodynamic instability may be suppressed for all but very long wavelength disturbances.

This treatment of the flame structure as an internal boundary layer in the hydrodynamic field has application to other premixed combustion systems as well. In particular, Kaper *et al.* (1985) have extended this type of analysis to a flame attached to a flameholder, the effects of which are capable of suppressing hydrodynamic instability for inflow velocities sufficiently less than the adiabatic flame speed. In the present work, we consider two types of multiphase systems consisting of a gas flame attached to a pyrolyzing solid or liquid propellant. If it is assumed that the multiphase flame, which includes the propellant interface, the multiphase preheat zone, and the gas-phase reaction zone, is thin compared to some characteristic length, then this multiphase flame can also be treated as an internal boundary layer separating the unburned condensed-phase propellant from the burned gas. Thus, in the appropriate limit, this boundary layer again becomes a surface of hydrodynamic discontinuity across which jump conditions on the fluid and transport variables may be derived.

Before proceeding, we remark that there exists another source of non-acoustic (small Mach number) combustion instability which is not related to the jump, due to thermal expansion, in the fluid variables across the reaction front. Rather, it stems from a reactive/diffusive instability associated with the highly nonlinear temperature sensitivity (as measured by the activation energy) of the reaction rate. Such instabilities, which can be either pulsating (nonsteady) or cellular (steady, but nonplanar) in nature, exist even in the limit of zero thermal expansion. Since these instabilities occur on diffusive time and spatial scales, they are effectively suppressed on the hydrodynamic scales of interest here, just as hydrodynamic instabilities are suppressed in the limit of zero thermal expansion. The two types of analyses overlap in the limit of weak thermal expansion and small wavenumber (long-wave) disturbances, in which case it is usually possible to derive a nonlinear evolution equation for the motion of the flame front (*cf.* Sivashinsky, 1983; Joulin and Sivashinsky, 1983; Margolis and Sivashinsky, 1984). There is a considerable literature on this non-hydrodynamic type of instability not only in gaseous combustion, where it is usually referred to as diffusional/thermal flame instability [see, for example, the review by Margolis and Matkowsky (1983) and the monograph by Buckmaster and Ludford (1983)], but also in condensed-phase combustion synthesis of refractory materials (*cf.* Merzhanov *et al.*, 1973; Matkowsky and Sivashinsky, 1978; Margolis, 1983; Margolis *et al.*, 1985; Booty *et al.*, 1986). More recently, new reactive/diffusive instabilities have been found in solid propellant combustion (Margolis and Armstrong, 1986; Margolis and Williams, 1988, 1989), and a generalization of the Landau model for liquid propellants to include a temperature and pressure dependence on the propagation rate shows that such instabilities can arise there as well (Armstrong and Margolis, 1989a,b). The present work thus complements these latter studies on propellant deflagration by investigating the role of hydrodynamic instability in these systems.

§2. The Mathematical Model

The model which we employ to describe both solid and liquid propellant combustion is similar to that introduced in Margolis and Armstrong (1986) and Margolis and Williams (1988, 1989) for solid propellants, and is sketched in Figure 1. We assume that there is no reaction in the liquid (solid) phase and that there exists a surface $\tilde{x}_3 = \tilde{\Phi}_p(\tilde{x}_1, \tilde{x}_2, \tilde{t})$ separating the condensed and gas phases. At this surface, a specified fraction $\alpha > 0$ of the propellant vaporizes (sublimes) and burns in the gas phase, while the remaining fraction $(1 - \alpha)$ is pyrolyzed directly into gaseous products. Both the pyrolysis and the gas-phase reactions are assumed to be governed by overall Arrhenius processes with large activation energies which are of the same order of magnitude.

We assume that within the gas and condensed phases separately, the heat capacity, thermal conductivity, mass diffusivity (assumed to be negligible in the condensed phase), and viscosity are constant, but we allow for jumps in these quantities across the phase boundary. In the previous studies of solid propellant combustion referred to above, the emphasis was on reactive/diffusive instabilities, and thus the density was also assumed to be constant in both phases. This assumption effectively decoupled the transport processes governing heat conduction and diffusion of chemical species from the underlying (unidirectional) velocity field, and permitted the analysis of diffusional/thermal influences on the overall intrinsic stability of solid propellant combustion. On the other hand, Armstrong and Margolis (1989a,b) allowed for such a coupling between the transport processes and the hydrodynamic field in their generalization of Landau's (1944) model of liquid propellant combustion with a nonreactive gas phase. This model was then used to study hydrodynamic and reactive/diffusive instabilities in the pyrolysis of liquid propellants in the absence of gas-phase thermal expansion. Consequently, the present study extends both of these propellant models by allowing for thermal expansion in a reactive gas phase, where the gas flame is located at a finite distance from the propellant surface. The variation of density in the gas phase and across the propellant surface thus allows for the full interaction among the transport processes and the flow fields in both phases. For the most part, we treat the solid and liquid propellant problems simultaneously, since both models are governed by the same conservation equations and interface conditions.

The full system of governing equations in the gas phase are given by

$$\frac{\partial \tilde{\rho}}{\partial \tilde{t}} + \tilde{\nabla} \cdot (\tilde{\rho} \tilde{\mathbf{V}}) = 0 \quad (2.1)$$

$$\tilde{\rho} \left\{ \frac{\partial \tilde{\mathbf{V}}}{\partial \tilde{t}} + \tilde{\mathbf{V}} \cdot \tilde{\nabla} \tilde{\mathbf{V}} \right\} = -\tilde{\nabla} \tilde{P} + \mu_g \left\{ \tilde{\nabla}^2 \tilde{\mathbf{V}} + \frac{1}{3} \tilde{\nabla} (\tilde{\nabla} \cdot \tilde{\mathbf{V}}) \right\} \quad (2.2)$$

$$\tilde{R}^0 \tilde{\rho} \tilde{T} = \tilde{P} \quad (2.3)$$

$$\tilde{\rho} \left\{ \frac{\partial Y}{\partial \tilde{t}} + \tilde{\mathbf{V}} \cdot \tilde{\nabla} Y \right\} = \tilde{\rho} \tilde{D} \tilde{\nabla}^2 Y - \tilde{A} Y^n \exp \left(-\frac{\tilde{E}}{\tilde{R}^0 \tilde{T}} \right) \quad (2.4)$$

$$\bar{\rho} \left\{ \frac{\partial \bar{T}}{\partial \bar{t}} + \bar{\mathbf{V}} \cdot \bar{\nabla} \bar{T} \right\} = \frac{\bar{\lambda}_g}{\bar{c}_g} \bar{\nabla}^2 \bar{T} + \frac{\bar{c}_p}{\bar{c}_g} (\bar{\beta} + \bar{\gamma}) \bar{A} Y^n \exp \left(-\frac{\bar{E}}{\bar{R}^0 \bar{T}} \right) \quad (2.5)$$

$$Y = 0, \quad \bar{T} = \bar{T}_a = \frac{\bar{c}_p}{\bar{c}_g} (\bar{T}_u + \bar{\beta}) \quad \text{at } \bar{x}_3 = \infty. \quad (2.6)$$

Here $\bar{\rho}$, $\bar{\mathbf{V}}$, \bar{P} , Y , and \bar{T} represent the density, velocity field, pressure, unreacted mass fraction, and temperature respectively of the gas phase. In these equations, $\bar{\mu}_g$, $\bar{\lambda}_g$, \bar{c}_g are the viscosity, thermal conductivity, and heat capacity in the gas phase, \bar{c}_p is the heat capacity of the propellant, \bar{D} is the mass diffusivity of the gas, $\bar{\gamma}$ is the heat of vaporization(sublimation) of the propellant, and $\bar{\beta}$ is the overall heat of reaction. These last two quantities are given in units of temperature through division by \bar{c}_p . The constant \bar{T}_u is the temperature far into the propellant (at $\bar{x}_3 = -\infty$), \bar{A} and \bar{E} are the rate coefficient and activation energy of the gas phase reaction, and \bar{R}^0 is the gas constant.

In the condensed phase, $\bar{x}_3 < \bar{\Phi}_p$,

$$Y = 1, \quad \bar{\rho} = \bar{\rho}_p \quad (2.7)$$

$$\bar{\nabla} \cdot \bar{\mathbf{V}} = 0 \quad (2.8)$$

$$\bar{\rho}_p \left\{ \frac{\partial \bar{\mathbf{V}}}{\partial \bar{t}} + \bar{\mathbf{V}} \cdot \bar{\nabla} \bar{\mathbf{V}} \right\} = -\bar{\nabla} \bar{P} + \mu_p \left\{ \bar{\nabla}^2 \bar{\mathbf{V}} + \frac{1}{3} \bar{\nabla} (\bar{\nabla} \cdot \bar{\mathbf{V}}) \right\} \quad (2.9)$$

$$\bar{\rho} \left\{ \frac{\partial \bar{T}}{\partial \bar{t}} + \bar{\mathbf{V}} \cdot \bar{\nabla} \bar{T} \right\} = \frac{\bar{\lambda}_p}{\bar{c}_p} \bar{\nabla}^2 \bar{T} \quad (2.10)$$

$$\bar{T} = \bar{T}_u \quad \text{at } \bar{x}_3 = -\infty, \quad (2.11)$$

where the subscript "p" is used to denote quantities in the propellant. For the case in which the propellant is a solid, there can be no motion in the condensed phase and thus

$$\bar{\mathbf{V}} \equiv 0 \quad \text{for } \bar{x}_3 < \bar{\Phi}_p. \quad (2.12)$$

This system of equations must be solved subject to appropriate boundary conditions at the propellant interface where the velocity $\bar{\mathbf{V}}_p$ in the \bar{x}_3 direction and the unit normal $\hat{\mathbf{n}}_p$ to the interface are given by

$$\bar{\mathbf{V}}_p = \left(0, 0, \frac{\partial \bar{\Phi}_p}{\partial \bar{t}} \right), \quad (2.13)$$

$$\hat{\mathbf{n}}_p = \left(-\frac{\partial \bar{\Phi}_p}{\partial \bar{x}_1}, -\frac{\partial \bar{\Phi}_p}{\partial \bar{x}_2}, 1 \right) \left[1 + \left(\frac{\partial \bar{\Phi}_p}{\partial \bar{x}_1} \right)^2 + \left(\frac{\partial \bar{\Phi}_p}{\partial \bar{x}_2} \right)^2 \right]^{-1/2}. \quad (2.14)$$

We require that the temperature be continuous across this surface, and, due to the action of viscosity, a no-slip condition is imposed. In addition, the mass flux normal to the interface must be continuous. Hence,

$$\bar{T}_- = \bar{T}_+ \quad (2.15)$$

$$\hat{\mathbf{n}}_p \times \bar{\mathbf{V}}_- = \hat{\mathbf{n}}_p \times \bar{\mathbf{V}}_+, \quad \bar{\rho}_p \hat{\mathbf{n}}_p \cdot (\bar{\mathbf{V}}_- - \bar{\mathbf{V}}_p) = \bar{\rho}_+ \hat{\mathbf{n}}_p \cdot (\bar{\mathbf{V}}_+ - \bar{\mathbf{V}}_p), \quad (2.16)$$

where a subscript \pm signifies evaluation at $\tilde{x}_3 = \tilde{\Phi}_p^\pm$. The mass burning rate is given by the pyrolysis law

$$\tilde{\rho}_p \hat{\mathbf{n}}_p \cdot (\tilde{\mathbf{V}}_- - \tilde{\mathbf{V}}_p) = \tilde{A}_p \exp(-\tilde{E}_p / \tilde{R}^0 \tilde{T}), \quad (2.17)$$

and conservation of flux of normal momentum across the interface determines the jump in the pressure field,

$$\begin{aligned} \tilde{P}_- - \tilde{P}_+ &= \tilde{\rho}_p [\hat{\mathbf{n}}_p \cdot (\tilde{\mathbf{V}}_- - \tilde{\mathbf{V}}_p)] \hat{\mathbf{n}}_p \cdot (\tilde{\mathbf{V}}_+ - \tilde{\mathbf{V}}_-) + \tilde{\gamma}^* \tilde{\nabla} \cdot \hat{\mathbf{n}}_p \\ &\quad - \mu_g \hat{\mathbf{n}}_p \cdot (\tilde{\mathbf{E}}_+ \hat{\mathbf{n}}_p) + \mu_p \hat{\mathbf{n}}_p \cdot (\tilde{\mathbf{E}}_- \hat{\mathbf{n}}_p), \end{aligned} \quad (2.18)$$

where $\tilde{\gamma}^*$ is the coefficient of surface tension for the liquid propellant or the coefficient of surface energy for the solid propellant. Here, the components $\tilde{e}_{i,j}$ of the rate of strain tensor $\tilde{\mathbf{E}}$ are given in terms of the components \tilde{v}_k of the velocity vector $\tilde{\mathbf{V}}$ by $\tilde{e}_{i,j} = \partial \tilde{v}_i / \partial \tilde{x}_j + \partial \tilde{v}_j / \partial \tilde{x}_i$. The curvature $-\tilde{\nabla} \cdot \hat{\mathbf{n}}_p$ of the interface is given in terms of $\tilde{\Phi}_p$ by

$$-\tilde{\nabla} \cdot \hat{\mathbf{n}}_p = \frac{\frac{\partial^2 \tilde{\Phi}_p}{\partial \tilde{x}_1^2} \left[1 + \left(\frac{\partial \tilde{\Phi}_p}{\partial \tilde{x}_2} \right)^2 \right] + \frac{\partial^2 \tilde{\Phi}_p}{\partial \tilde{x}_2^2} \left[1 + \left(\frac{\partial \tilde{\Phi}_p}{\partial \tilde{x}_1} \right)^2 \right] - 2 \frac{\partial \tilde{\Phi}_p}{\partial \tilde{x}_1} \frac{\partial \tilde{\Phi}_p}{\partial \tilde{x}_2} \frac{\partial^2 \tilde{\Phi}_p}{\partial \tilde{x}_1 \partial \tilde{x}_2}}{\left[1 + \left(\frac{\partial \tilde{\Phi}_p}{\partial \tilde{x}_1} \right)^2 + \left(\frac{\partial \tilde{\Phi}_p}{\partial \tilde{x}_2} \right)^2 \right]^{3/2}}. \quad (2.19)$$

The conservation of flux of the tangential components of momentum gives

$$\mu_g \hat{\mathbf{n}}_p \times (\tilde{\mathbf{E}}_+ \hat{\mathbf{n}}_p) = \mu_p \hat{\mathbf{n}}_p \times (\tilde{\mathbf{E}}_- \hat{\mathbf{n}}_p), \quad (2.20)$$

and in addition there is conservation of heat flux

$$\begin{aligned} \hat{\mathbf{n}}_p \cdot (\tilde{\lambda}_g \tilde{\nabla} \tilde{T}_+ - \tilde{\lambda}_p \tilde{\nabla} \tilde{T}_-) &= \tilde{c}_g \tilde{\rho}_+ \hat{\mathbf{n}}_p \cdot (\tilde{\mathbf{V}}_+ - \tilde{\mathbf{V}}_p) \tilde{T}_+ - \tilde{c}_p \tilde{\rho}_p \hat{\mathbf{n}}_p \cdot (\tilde{\mathbf{V}}_- - \tilde{\mathbf{V}}_p) \tilde{T}_- \\ &\quad + \tilde{c}_p \tilde{\rho}_p \hat{\mathbf{n}}_p \cdot (\tilde{\mathbf{V}}_p - \tilde{\mathbf{V}}_-) [-\alpha \tilde{\gamma} + (1 - \alpha) \tilde{\beta}] \end{aligned} \quad (2.21)$$

and conservation of unreacted mass flux

$$\tilde{\rho}_+ \tilde{D} \hat{\mathbf{n}}_p \cdot \tilde{\nabla} Y_+ = \tilde{\rho}_+ \hat{\mathbf{n}}_p \cdot (\tilde{\mathbf{V}}_+ - \tilde{\mathbf{V}}_p) Y_+ + \alpha \tilde{\rho}_p \hat{\mathbf{n}}_p \cdot \tilde{\mathbf{V}}_p. \quad (2.22)$$

We nondimensionalize temperature, velocities and pressure with respect to \tilde{T}_a , \tilde{U} and \tilde{P}_∞ , which denote the flame temperature, propagation velocity of the propellant surface, and the pressure in the burned gas, respectively, for the case of planar, adiabatic combustion. In addition, $\tilde{\rho}_p$ serves as a unit for the density. The diffusion process introduces the length and time scales

$$l_D = \frac{\tilde{\lambda}_p}{\tilde{\rho}_p \tilde{c}_p \tilde{U}}, \quad t_* = \frac{l_D}{\tilde{U}}, \quad (2.23)$$

but since our focus here is on hydrodynamic instability, we follow the same approach as that of Matlon and Matkowsky (1982) and scale distances on a characteristic length L of the hydrodynamic field, such as the wavelength of a disturbance, and time on L/\tilde{U} . The ratio

$$\delta \equiv \frac{l_D}{L} \quad (2.24)$$

thus represents the relative thickness of the multiphase flame, which includes the propellant interface, the multiphase preheat zone, and the gas-phase reaction zone. The gas-phase activation energy is scaled on $\bar{R}^0 \bar{T}_a$ and this gives rise to the nondimensional parameter

$$N = \frac{\bar{E}}{\bar{R}^0 \bar{T}_a}. \quad (2.25)$$

When N is large, the reaction rate is strongly temperature dependent and the reaction is confined to a thin region (relative to the preheat zone) which is referred to as the gas-phase reaction zone. In the following section we will exploit this limit, which will allow this thin layer to be approximated by a surface $x_3 = \Phi_r$ separating burned from unburned gases. It is thus convenient to adopt a coordinate system moving with the reaction zone

$$x = x_1, \quad y = x_2, \quad z = x_3 - \Phi_r(x_1, x_2, t) \quad (2.26)$$

so that the propellant interface is located at the position

$$z_0(x_1, x_2, t) \equiv \Phi_p(x_1, x_2, t) - \Phi_r(x_1, x_2, t) < 0. \quad (2.27)$$

Employing these nondimensionalizations and the moving coordinate system (2.26), we obtain the nondimensional gas-phase equations

$$\frac{\partial \rho}{\partial t} + \frac{\partial M}{\partial z} + \nabla \cdot (\rho \mathbf{v}) = 0 \quad (2.28)$$

$$\rho \frac{\partial \mathbf{v}}{\partial t} + M \frac{\partial \mathbf{v}}{\partial z} + \rho \mathbf{v} \cdot \nabla \mathbf{v} = -\nabla p + \nabla \Phi_r \frac{\partial p}{\partial z} + \delta P r_g \left\{ \Delta \mathbf{v} + \frac{1}{3} \left(\nabla - \nabla \frac{\partial}{\partial z} \right) \left(\frac{\partial s}{\partial z} + \nabla \cdot \mathbf{v} \right) \right\} \quad (2.29)$$

$$\rho \frac{\partial w}{\partial t} + M \frac{\partial w}{\partial z} + \rho \mathbf{v} \cdot \nabla w = -\frac{\partial p}{\partial z} + \delta P r_g \left\{ \Delta w + \frac{1}{3} \frac{\partial}{\partial z} \left(\frac{\partial s}{\partial z} + \nabla \cdot \mathbf{v} \right) \right\} \quad (2.30)$$

$$\rho T = \rho_\infty \quad (2.31)$$

$$\rho \frac{\partial Y}{\partial t} + M \frac{\partial Y}{\partial z} + \rho \mathbf{v} \cdot \nabla Y - \delta \frac{\lambda}{c l e} \Delta Y = -\delta \Omega \quad (2.32)$$

$$\rho \frac{\partial T}{\partial t} + M \frac{\partial T}{\partial z} + \rho \mathbf{v} \cdot \nabla T - \delta \frac{\lambda}{c} \Delta T = \beta \delta \Omega \quad (2.33)$$

$$Y = 0 \quad \text{for } z > \Phi_r, \quad (2.34)$$

while in the condensed phase,

$$\rho = Y = 1 \quad (2.35)$$

$$\frac{\partial M}{\partial z} + \nabla \cdot \mathbf{v} = 0 \quad (2.36)$$

$$\frac{\partial \mathbf{v}}{\partial t} + M \frac{\partial \mathbf{v}}{\partial z} + \mathbf{v} \cdot \nabla \mathbf{v} = -\nabla p + \nabla \Phi_r \frac{\partial p}{\partial z} + \delta P r_l \left\{ \Delta \mathbf{v} + \frac{1}{3} \left(\nabla - \nabla \frac{\partial}{\partial z} \right) \left(\frac{\partial s}{\partial z} + \nabla \cdot \mathbf{v} \right) \right\} \quad (2.37)$$

$$\frac{\partial w}{\partial t} + M \frac{\partial w}{\partial z} + \mathbf{v} \cdot \nabla w = -\frac{\partial p}{\partial z} + \delta P r_l \left\{ \Delta w + \frac{1}{3} \frac{\partial}{\partial z} \left(\frac{\partial s}{\partial z} + \nabla \cdot \mathbf{v} \right) \right\} \quad (2.38)$$

$$\frac{\partial T}{\partial t} + M \frac{\partial T}{\partial z} + \mathbf{v} \cdot \nabla T - \delta \Delta T = 0 \quad (2.39)$$

$$T = \sigma, \quad \mathbf{V} = 0 \text{ at } z = -\infty \quad (2.40)$$

(for the case of a solid propellant, $\mathbf{V} \equiv 0$ in the solid phase). In these equations, we have introduced the two-dimensional transverse gradient $\nabla \equiv (\partial/\partial x; \partial/\partial y)$, in terms of which the Laplacian Δ in this coordinate system is given by

$$\Delta = \left[1 + (\nabla \Phi_r)^2\right] \frac{\partial^2}{\partial z^2} + \nabla^2 - \nabla^2 \Phi_r \frac{\partial}{\partial z} - 2 \frac{\partial}{\partial z} (\nabla \Phi_r \cdot \nabla). \quad (2.41)$$

In addition, we have decomposed the velocity field according to $\mathbf{V} = \mathbf{v} + w\mathbf{k}$, where \mathbf{k} is the unit vector normal to the gas-phase reaction front $x_3 = \Phi_r$ and $\mathbf{v} \cdot \mathbf{k} = 0$, and have introduced the notation

$$\rho s = M = \rho \left\{ w - \mathbf{v} \cdot \nabla \Phi_r - \frac{\partial \Phi_r}{\partial t} \right\}. \quad (2.42)$$

The reaction rate term Ω appearing in the transport equations is given by

$$\Omega = \Lambda A(T) Y^n \exp \left[N \left(1 - \frac{1}{T} \right) \right] \quad (2.43)$$

where

$$A(T) = \tilde{A}(\tilde{T}) / \tilde{A}(\tilde{T}_a), \quad \Lambda = \frac{\tilde{\lambda}_p \tilde{A}(\tilde{T}_a)}{\delta^2 \tilde{c}_p \tilde{\rho}_p^2 \tilde{U}^2} \exp(-N). \quad (2.44)$$

Finally, the nondimensional parameters appearing in these equations include

$$\sigma = \frac{\tilde{T}_u}{\tilde{T}_a}, \quad \rho_\infty = \frac{\tilde{\rho}_\infty}{\tilde{\rho}_p}, \quad \lambda = \frac{\tilde{\lambda}_g}{\tilde{\lambda}_p}, \quad c = \frac{\tilde{c}_g}{\tilde{c}_p},$$

$$Le = \frac{\tilde{\lambda}_g}{\tilde{\rho}_\infty \tilde{D}_\infty \tilde{c}_g}, \quad Pr_{g(l)} = \frac{\mu_{g(l)} \tilde{c}_g}{\tilde{\lambda}_g}, \quad \beta = \frac{(c - \sigma)(1 + \tilde{\gamma}/\tilde{\beta})}{c} \quad (2.45)$$

where the Lewis number Le is the measure of thermal to mass diffusivity of the gas, and the Prandtl number Pr is the ratio of viscous to thermal effects. We remark here that an additional parameter, namely the Mach number, $Ma = \tilde{U} \sqrt{\tilde{\rho}_\infty / \tilde{P}_\infty}$, appears during the course of nondimensionalization. However, we will assume that the combustion front propagates at speeds much smaller than the speed of sound ($Ma \ll 1$) so that the total nondimensional pressure $P = 1 + Ma^2 p$ can be approximated as a constant in Eq. (2.3), resulting in the simplified equation of state (2.31). On the other hand, the gradient of pressure cannot be neglected, and thus appears in the momentum equations (2.29) - (2.30), (2.37) - (2.38).

Before writing down the boundary conditions at the propellant surface we introduce the additional nondimensional parameters

$$\sigma_p = \frac{\tilde{T}_p}{\tilde{T}_a}, \quad N_p = \frac{\tilde{E}_p}{\tilde{R}^0 \tilde{T}_p}, \quad A_p = \frac{\tilde{A}_p(\tilde{T})}{\tilde{A}_p(\tilde{T}_p)},$$

$$\Lambda_p = \frac{\tilde{A}_p(\tilde{T}_p)}{\tilde{\rho}_p \tilde{U}} \exp(-N_p), \quad \gamma = \frac{\gamma^* \tilde{c}_p}{\tilde{U} \tilde{\lambda}_p} \quad (2.46)$$

where \tilde{T}_p is the propellant surface temperature for steady, planar combustion. This quantity, as well as the burning velocity \tilde{U} , are determined as part of the steady, planar analysis to be considered in the next section. It is also convenient to introduce the notation

$$M_p = \rho \left\{ w - \mathbf{v} \cdot \nabla \Phi_p - \frac{\partial \Phi_p}{\partial t} \right\}, \quad (2.47)$$

for the longitudinal mass flux relative to the propellant surface. The boundary conditions at this surface are thus given by

$$T_- = T_+ \quad (2.48)$$

$$\rho_+ \hat{\mathbf{n}}_p \cdot (\mathbf{V}_+ - \mathbf{V}_p) = \hat{\mathbf{n}}_p \cdot (\mathbf{V}_- - \mathbf{V}_p) \quad (2.49)$$

$$\hat{\mathbf{n}}_p \times \mathbf{V}_+ = \hat{\mathbf{n}}_p \times \mathbf{V}_- \quad (2.50)$$

$$\hat{\mathbf{n}}_p \cdot (\mathbf{V}_- - \mathbf{V}_p) = A_p(T) \Lambda_p \exp \left[N_p \left(1 - \frac{\sigma_p}{T} \right) \right] \quad (2.51)$$

$$p_- - p_+ = M_p \left\{ 1 + |\nabla \Phi_p|^2 \right\}^{-1/2} \hat{\mathbf{n}}_p \cdot (\mathbf{V}_+ - \mathbf{V}_-) - \delta \gamma \nabla \cdot \frac{\nabla \Phi_p}{\{1 + |\nabla \Phi_p|^2\}^{1/2}} - \delta \frac{\lambda}{c} \hat{\mathbf{n}}_p \cdot (Pr_g \mathbf{E}_+ \hat{\mathbf{n}}_p - Pr_l \mathbf{E}_- \hat{\mathbf{n}}_p) \quad (2.52)$$

$$\hat{\mathbf{n}}_p \times (Pr_g \mathbf{E}_+ \hat{\mathbf{n}}_p - Pr_l \mathbf{E}_- \hat{\mathbf{n}}_p) = 0 \quad (2.53)$$

$$-M_p [(1-c)T_+ - \sigma + c(1-\alpha\beta)] = \delta \left\{ \lambda [(1 + \nabla \Phi_p \cdot \nabla \Phi_r) T_z - \nabla \Phi_p \cdot \nabla T]_+ - [(1 + \nabla \Phi_p \cdot \nabla \Phi_r) T_z - \nabla \Phi_p \cdot \nabla T]_- \right\} \quad (2.54)$$

$$M_p (Y_+ - \alpha) = \delta \frac{\lambda}{cLe} \left\{ (1 + \nabla \Phi_p \cdot \nabla \Phi_r) Y_z - \nabla \Phi_p \cdot \nabla Y \right\}_+ \quad (2.55)$$

We note that for the case of a solid propellant, $\mathbf{V}_- = \mathbf{E}_- = 0$ in these conditions.

§3. The Gas-Phase Reaction Zone

In general, we consider the limit $N \gg 1/\delta$, although we do not as yet make any assumptions on the magnitude of δ , which is simply regarded as an $O(1)$ parameter in this section. In this limit the reaction rate, Ω , becomes negligible except in a very thin region near $z = 0$. The analysis consists of stretching this region by introducing a new variable $\xi = Nz$, and seeking expansions of the form

$$T = T_0 + \frac{1}{N} T_1 + \frac{1}{N^2} T_2 + \dots, \quad Y = Y_0 + \frac{1}{N} Y_1 + \frac{1}{N^2} Y_2 + \dots, \quad (3.1)$$

and similarly for the remaining variables. The resulting systems of equations are solved recursively in powers of $1/N$, and the solutions are matched to the regions on either side of $z = 0$ where the reaction rate is negligible. The net result is to replace the nonlinear reaction term Ω by jump

conditions relating the transport and fluid variables across the surface $z = 0$. We will omit the details of this analysis since it is a synthesis of the analyses of Matkowsky and Sivashinsky (1979) and Matalon and Matkowsky (1982) for a gaseous flame, and that of Margolis and Williams (1988) for the transport variables in solid propellant combustion. This procedure results in a set of jump conditions across $z = 0$ which are given by

$$[T] = [Y] = [w] = [\mathbf{V}] = 0, \quad (3.2)$$

$$\left[\frac{\partial T}{\partial z} \right] = -\frac{\beta}{Le} \left[\frac{\partial Y}{\partial z} \right] \quad (3.3)$$

$$\left\{ 1 + |\nabla \Phi_r|^2 \right\}^{1/2} \left[\frac{\partial T}{\partial z} \right] = - \left(\frac{2c\Lambda\beta^{1-n}Le^n n!}{\lambda N^{n+1}} \right)^{1/2} \exp \left\{ \frac{N}{2}(T_+ - 1) \right\} = -\frac{\alpha\beta c}{\delta\lambda} \exp \left\{ \frac{N}{2}(T_+ - 1) \right\} \quad (3.4)$$

$$\left[\frac{\partial \mathbf{v}}{\partial z} + \nabla \Phi_r \frac{\partial w}{\partial z} \right] = 0, \quad (3.5)$$

$$[p] = \delta \frac{4}{3} Pr_g \frac{\lambda}{c} \left\{ 1 + |\nabla \Phi_r|^2 \right\} \left[\frac{\partial w}{\partial z} \right], \quad (3.6)$$

where $[\phi(z)] \equiv \phi(z = 0^+) - \phi(z = 0^-)$, and the second equality in Eq. (3.4) is obtained from the expression for the steady, planar burning rate eigenvalue Λ (Section 4).

We observe that the parameter N appears in the jump condition (3.4), which is a consequence of truncating our expansion for T according to

$$T = \begin{cases} T_0 & z < 0 \\ 1 + T_1/N & z > 0, \end{cases}$$

and replacing T_1 by $N(T_+ - 1)$ in (3.4); the remaining variables are truncated after the first term in their respective expansions (*e.g.*, $Y = Y_0$). This truncation procedure, which has also been applied in studies involving certain kinds of burner flames (Sivashinsky, 1975; Margolis, 1980), condensed phase combustion (Sivashinsky, 1981; Margolis, 1983, 1985) and solid propellant deflagration (Margolis and Armstrong, 1986; Margolis and Williams, 1988), results in a closed model for the transport variables.

In what follows, we will eventually exploit the limit $\delta \ll 1$ (Section 5), in which case the width of the multiphase preheat zone, though $O(\delta)$ on the hydrodynamic scale, is still large compared to the width of the gas-phase reaction zone. Consequently, the latter zone will always be regarded as a surface across which the variables satisfy the jump conditions (3.2) - (3.6).

§4. Steady Planar Deflagration

There exists a steady, one-dimensional solution of the governing equations (2.28)-(2.40) which satisfies the boundary conditions (2.48)-(2.55) and the jump conditions (3.2)-(3.6). This solution,

which is obtained for arbitrary values of δ and is valid for both solid and liquid propellant combustion, is given by

$$\Phi_r^0 = -t, \quad \Phi_p^0 = -t + z_0^0, \quad (4.1)$$

$$Y^0 = \begin{cases} 1 & z < z_0^0 \\ -\alpha(e^{cLe^z/\delta\lambda} - 1) & z_0^0 < z < 0 \\ 0 & z > 0 \end{cases} \quad (4.2)$$

$$T^0 = \begin{cases} \sigma + (\sigma_p - \sigma)e^{(z-z_0^0)/\delta} & z < z_0^0 \\ 1 + \alpha\beta(e^{cz/\delta\lambda} - 1) & z_0^0 < z < 0 \\ 1 & z > 0 \end{cases} \quad (4.3)$$

$$\rho^0 = \begin{cases} 1 & z < z_0^0 \\ \rho_\infty[1 + \alpha\beta(e^{cz/\delta\lambda} - 1)]^{-1} & z_0^0 < z < 0 \\ \rho_\infty & z > 0 \end{cases} \quad (4.4)$$

$$w^0 = \begin{cases} 0 & z < z_0^0 \\ \rho_\infty^{-1} - 1 + \alpha\beta\rho_\infty^{-1}(e^{cz/\delta\lambda} - 1) & z_0^0 < z < 0 \\ \rho_\infty^{-1} - 1 & z > 0 \end{cases} \quad (4.5)$$

$$p^0 = \begin{cases} \rho_\infty^{-1} - 1 & z < z_0^0 \\ \frac{4}{3}\alpha\beta\rho_\infty^{-1}Pr_g e^{cz/\delta\lambda} & z_0^0 < z < 0 \\ 0 & z > 0, \end{cases} \quad (4.6)$$

where the superscript "0" is used to denote the steady, planar solution. The distance z_0^0 of the flame sheet from the propellant/gas interface is given in terms of the surface temperature σ_p , which is to be determined, by

$$z_0^0 = \delta \frac{\lambda}{c} \ln \left\{ \frac{\sigma_p - 1 + \alpha\beta}{\alpha\beta} \right\}. \quad (4.7)$$

Since positive values of z_0^0 are unphysical, it is clear from (4.7) that σ_p must be restricted to lie in the range $1 - \alpha\beta < \sigma_p < 1$ in order for a steady, planar deflagration to exist. In the limit that the surface temperature approaches the burned gas temperature ($\sigma_p \rightarrow 1$), the gas phase reaction zone approaches the propellant interface ($z_0^0 \rightarrow 0$), and the gaseous preheat zone disappears. In this intrusive limit, the present analysis does not apply and a separate analysis is required (cf. Margolis and Armstrong, 1986). Also, on physical grounds, one certainly expects the condensed propellant to be more dense than the gas. The result (4.4) reveals that the gas-phase density decreases monotonically from its value at the interface, $\rho^0 = \rho_\infty/\sigma_p$, to its constant value ρ_∞ in the burned gas. Consequently, in the following, we will only consider parameter values lying in the range $\rho_\infty < \rho_\infty/\sigma_p < 1$. Finally, the steady, planar analysis provides us with expressions for the burning rate eigenvalue Λ , from which Eq. (2.44) gives the dimensional burning velocity \bar{U} , and the dimensional surface temperature \bar{T}_p . In particular, we obtain

$$\bar{U} = \left\{ \frac{2n!Le^n \bar{A}(\bar{T}_a) \bar{\lambda}_g}{\bar{c}_g \bar{\rho}_p^2 N^{n+1} \alpha^2 \beta^{n+1}} \right\}^{1/2} e^{-N/2}, \quad (4.8)$$

$$\sigma_p = \tilde{T}_p/\tilde{T}_a = 2 \frac{\tilde{E}_p}{\tilde{E}_g} \left[1 + \frac{\tilde{R}^0 \tilde{T}_a}{\tilde{E}_g} \ln \left(\frac{\tilde{A}_p^2 \tilde{c}_g N^{n+1} \alpha^2 \beta^{n+1}}{\tilde{A}(\tilde{T}_a) 2n! \tilde{\lambda}_g L e^n} \right) \right]^{-1}. \quad (4.9)$$

In writing (4.9) as an explicit expression determining σ_p , we have assumed that the rate coefficient \tilde{A}_p is independent of temperature, so that A_p in the pyrolysis law (2.51) will be taken to be unity.

We recall that the above steady, planar solution was obtained without making any assumptions on the magnitude of δ . However, in the following sections we will consider the more general case of nonsteady, nonplanar combustion, and exploit the limit $\delta \ll 1$, in which case we obtain from Eq. (4.7) that $z_0^0 = O(\delta)$. Thus on a hydrodynamic scale, the propellant surface, the multiphase preheat zone, and the very thin gas-phase reaction zone (surface) all lie within the same narrow region.

§5. The Multiphase Flame

We now consider the limit $\delta \ll 1$. Thus viscous dissipation, heat conduction, and species diffusion, as well as the gas-phase reaction zone and propellant/gas interface are all confined to a thin $O(\delta)$ region which we call the multiphase flame. In the limit $\delta \rightarrow 0$, the flame shrinks to the surface $z = 0$, and on both sides of the flame we seek outer solutions to our system of the form

$$\begin{aligned} T &= T_0 + \delta T_1 + \dots, & \rho &= R_0 + \delta R_1 + \dots, \\ w &= W_0 + \delta W_1 + \dots, & \mathbf{v} &= \mathbf{V}_0 + \delta \mathbf{V}_1 + \dots, \\ p &= P_0 + \delta P_1 + \dots, & \Phi_r &= \Phi_{r,0} + \delta \Phi_{r,1} + \dots, \\ M &= M_0 + \delta M_1 + \dots, & M_p &= M_{p,0} + \delta M_{p,1} + \dots, \\ \Phi_p &= \Phi_{p,0} + \delta \Phi_{p,1} + \dots, & z_0 &= \delta f_1 + \dots = \delta(\Phi_{p,1} - \Phi_{r,1}) + \dots, \end{aligned} \quad (5.1)$$

with

$$Y \equiv \begin{cases} 1 & z < 0 \\ 0 & z > 0. \end{cases} \quad (5.2)$$

In order to relate these variables across the surface $z = 0$ as well as to obtain an equation describing the dynamics of the front itself, it is necessary to examine the multiphase flame structure. Analyses of this kind have been performed previously for the case of freely propagating gas flames (Matalon and Matkowsky, 1982) and for gas flames attached to a flameholder (Kaper, et.al., 1985) in order to derive conditions relating the fluid variables across the flame.

To study the structure, we introduce the stretched variable $z = \delta \zeta$ and seek inner solutions of the form

$$\begin{aligned} T &= \theta_0 + \delta \theta_1 + \dots, & \rho &= \rho_0 + \delta \rho_1 + \dots, \\ w &= w_0 + \delta w_1 + \dots, & \mathbf{v} &= \mathbf{v}_0 + \delta \mathbf{v}_1 + \dots, \end{aligned}$$

$$\begin{aligned}
M &= m_0 + \delta m_1 + \dots, & M_p &= m_{p,0} + \delta m_{p,1} + \dots, \\
p &= p_0 + \delta p_1 + \dots, & Y &= Y_0 + \delta Y_1 + \dots.
\end{aligned} \tag{5.3}$$

These expansions are now inserted into the governing equations, the boundary conditions at the interface $\zeta = f_1 + \dots$, and the jump conditions at the reaction zone $\zeta = 0$ to yield a system of equations to be solved recursively for the coefficients in the expansions (5.3). Upon solving for these coefficients, they are then evaluated as $\zeta \rightarrow \pm\infty$ to obtain matching conditions for the outer variables (5.1). In the remainder of this section, we consider the leading-order structure problem, deferring consideration of higher-order terms until later (Sections 6.2 and 7).

§5.1. Structure Analysis to Leading Order

As a result of our scaling for z_0 , which implied that $\Phi_{p,0} = \Phi_{r,0}$, we obtain to leading order the gas-phase equations ($f_1 < \zeta < 0$, $0 < \zeta < \infty$),

$$\rho_0 \theta_0 = \rho_\infty \tag{5.4}$$

$$\frac{\partial m_0}{\partial \zeta} = 0 \tag{5.5}$$

$$m_0 \frac{\partial \theta_0}{\partial \zeta} - \frac{\lambda}{c} (1 + |\nabla \Phi_{r,0}|^2) \frac{\partial^2 \theta_0}{\partial \zeta^2} = 0 \tag{5.6}$$

$$m_0 \frac{\partial Y_0}{\partial \zeta} - \frac{\lambda}{c Le} (1 + |\nabla \Phi_{r,0}|^2) \frac{\partial^2 Y_0}{\partial \zeta^2} = 0, \quad Y_0 \equiv 0 \text{ for } \zeta > 0 \tag{5.7}$$

$$m_0 \frac{\partial w_0}{\partial \zeta} - \frac{\lambda}{c} Pr_g \left\{ (1 + |\nabla \Phi_{r,0}|^2) \frac{\partial^2 w_0}{\partial \zeta^2} + \frac{1}{3} \left(\frac{\partial^2 w_0}{\partial \zeta^2} - \nabla \Phi_{r,0} \cdot \frac{\partial^2 \mathbf{v}_0}{\partial \zeta^2} \right) \right\} = -\frac{\partial p_0}{\partial \zeta} \tag{5.8}$$

$$m_0 \frac{\partial \mathbf{v}_0}{\partial \zeta} - \frac{\lambda}{c} Pr_g \left\{ (1 + |\nabla \Phi_{r,0}|^2) \frac{\partial^2 \mathbf{v}_0}{\partial \zeta^2} + \frac{1}{3} \left(\frac{\partial^2 w_0}{\partial \zeta^2} - \nabla \Phi_{r,0} \cdot \frac{\partial^2 \mathbf{v}_0}{\partial \zeta^2} \right) \right\} = \nabla \Phi_{r,0} \frac{\partial p_0}{\partial \zeta}, \tag{5.9}$$

and the condensed phase equations ($-\infty < \zeta < f_1$),

$$\rho_0 = Y_0 = 1 \tag{5.10}$$

$$\frac{\partial m_0}{\partial \zeta} = 0 \tag{5.11}$$

$$m_0 \frac{\partial \theta_0}{\partial \zeta} - (1 + |\nabla \Phi_{r,0}|^2) \frac{\partial^2 \theta_0}{\partial \zeta^2} = 0 \tag{5.12}$$

$$m_0 \frac{\partial w_0}{\partial \zeta} - \frac{\lambda}{c} Pr_l \left\{ (1 + |\nabla \Phi_{r,0}|^2) \frac{\partial^2 w_0}{\partial \zeta^2} + \frac{1}{3} \left(\frac{\partial^2 w_0}{\partial \zeta^2} - \nabla \Phi_{r,0} \cdot \frac{\partial^2 \mathbf{v}_0}{\partial \zeta^2} \right) \right\} = -\frac{\partial p_0}{\partial \zeta} \tag{5.13}$$

$$m_0 \frac{\partial \mathbf{v}_0}{\partial \zeta} - \frac{\lambda}{c} Pr_l \left\{ (1 + |\nabla \Phi_{r,0}|^2) \frac{\partial^2 \mathbf{v}_0}{\partial \zeta^2} + \frac{1}{3} \left(\frac{\partial^2 w_0}{\partial \zeta^2} - \nabla \Phi_{r,0} \cdot \frac{\partial^2 \mathbf{v}_0}{\partial \zeta^2} \right) \right\} = \nabla \Phi_{r,0} \frac{\partial p_0}{\partial \zeta}, \tag{5.14}$$

where $\mathbf{v}_0 = w_0 = 0$ for the solid propellant. In addition, the jump conditions across the gas-phase reaction front at $\zeta = 0$ are obtained from Eqs. (3.2) - (3.6) as

$$[\theta_0] = [Y_0] = [w_0] = [\mathbf{V}_0] = 0, \quad (5.15)$$

$$\left[\frac{\partial \theta_0}{\partial \zeta} \right] = -\frac{\beta}{Le} \left[\frac{\partial Y_0}{\partial \zeta} \right] \quad (5.16)$$

$$\left\{ 1 + |\nabla \Phi_{r,0}|^2 \right\}^{1/2} \left[\frac{\partial \theta_0}{\partial \zeta} \right] = -\alpha \beta c \lambda^{-1} \exp \left\{ \frac{N}{2} (\theta_0(0^+) - 1) \right\}, \quad (5.17)$$

$$\left[\frac{\partial \mathbf{v}_0}{\partial \zeta} + \nabla \Phi_{r,0} \frac{\partial w_0}{\partial \zeta} \right] = 0, \quad (5.18)$$

$$[p_0] = \frac{4}{3} Pr_g \frac{\lambda}{c} \left\{ 1 + |\nabla \Phi_{r,0}|^2 \right\} \left[\frac{\partial w_0}{\partial \zeta} \right], \quad (5.19)$$

and the boundary conditions at the interface $\zeta = f_1$ are

$$[[m_{p,0}]] = [[m_0]] = [[\theta_0]] = 0 \quad (5.20)$$

$$m_{p,0}|_{\zeta=f_1} = \left(1 + |\nabla \Phi_{r,0}|^2 \right)^{1/2} \exp \left\{ N_p \left(1 - \frac{\sigma_p}{\theta_0} \right) \right\} \quad (5.21)$$

$$\left\{ (c-1)\theta_0^+ + \sigma - c(1-\alpha\beta) \right\} m_{p,0}|_{\zeta=f_1} = \left(1 + |\nabla \Phi_{r,0}|^2 \right) \left(\lambda \frac{\partial \theta_0^+}{\partial \zeta} - \frac{\partial \theta_0^-}{\partial \zeta} \right) \quad (5.22)$$

$$(Y_0^+ - \alpha) m_{p,0}|_{\zeta=f_1} = \frac{\lambda}{c Le} \left(1 + |\nabla \Phi_{r,0}|^2 \right) \frac{\partial Y_0^+}{\partial \zeta} \quad (5.23)$$

$$[[\mathbf{v}_0 + \nabla \Phi_{r,0} w_0]] = 0 \quad (5.24)$$

$$Pr_g \left(\frac{\partial \mathbf{v}_0}{\partial \zeta} + \nabla \Phi_{r,0} \frac{\partial w_0}{\partial \zeta} \right)^+ = Pr_l \left(\frac{\partial \mathbf{v}_0}{\partial \zeta} + \nabla \Phi_{r,0} \frac{\partial w_0}{\partial \zeta} \right)^- \quad (5.25)$$

$$-[[p_0]] = \left\{ 1 + |\nabla \Phi_{r,0}|^2 \right\}^{-1} \left\{ [[w_0 - \nabla \Phi_{r,0} \cdot \mathbf{v}_0]] m_{p,0}|_{\zeta=f_1} - \frac{4\lambda}{3c} \left\{ Pr_g \left(\frac{\partial w_0}{\partial \zeta} - \nabla \Phi_{r,0} \cdot \frac{\partial \mathbf{v}_0}{\partial \zeta} \right)^+ - Pr_l \left(\frac{\partial w_0}{\partial \zeta} - \nabla \Phi_{r,0} \cdot \frac{\partial \mathbf{v}_0}{\partial \zeta} \right)^- \right\} \right\}, \quad (5.26)$$

where $[[\phi(\zeta)]] = \phi(\zeta = f_1^+) - \phi(\zeta = f_1^-)$ and a superscript \pm signifies evaluation at $\zeta = f_1^\pm$. Thus, the chosen length and time scales reduce the original system of partial differential equations to a system of ordinary differential equations within the structure. The matching conditions for $\zeta \rightarrow \pm\infty$ then serve to completely determine these solutions, which are given by

$$m_0 = m_{p,0} = \left(1 + |\nabla \Phi_{r,0}|^2 \right)^{1/2} \quad (5.27)$$

$$Y_0 = \begin{cases} 1 & \zeta < f_1 \\ -\alpha(e^{c Le \zeta / \lambda m_0} - 1) & f_1 < \zeta < 0 \\ 0 & \zeta > 0 \end{cases} \quad (5.28)$$

$$\theta_0 = \begin{cases} \sigma + (\sigma_p - \sigma)e^{(\zeta - f_1)} & \zeta < f_1 \\ 1 + \alpha\beta(e^{c\zeta/\lambda m_0} - 1) & f_1 < \zeta < 0 \\ 1 & \zeta > 0 \end{cases} \quad (5.29)$$

$$\rho_0 = \begin{cases} 1 & \zeta < f_1 \\ \rho_\infty [1 + \alpha\beta(e^{c\zeta/\lambda m_0} - 1)]^{-1} & f_1 < \zeta < 0 \\ \rho_\infty & \zeta > 0 \end{cases} \quad (5.30)$$

$$w_0 = \begin{cases} W_0(0^+) - m_0^{-1}\rho_\infty^{-1} - 1 & \zeta < f_1 \\ W_0(0^+) + \alpha\beta\rho_\infty^{-1}m_0^{-1}(e^{c\zeta/\lambda m_0} - 1) & f_1 < \zeta < 0 \\ W_0(0^+) & \zeta > 0 \end{cases} \quad (5.31)$$

$$v_0 = \begin{cases} V_0(0^+) + \nabla\Phi_{r,0}(\rho_\infty^{-1} - 1)m_0^{-1} & \zeta < f_1 \\ V_0(0^+) - \nabla\Phi_{r,0}\alpha\beta\rho_\infty^{-1}m_0^{-1}(e^{c\zeta/\lambda m_0} - 1) & f_1 < \zeta < 0 \\ V_0(0^+) & \zeta > 0 \end{cases} \quad (5.32)$$

$$p_0 = \begin{cases} P_0(0^+) + \rho_\infty^{-1} - 1 & \zeta < f_1 \\ P_0(0^+) + \alpha\beta\rho_\infty^{-1} + \alpha\beta\rho_\infty^{-1}e^{c\zeta/\lambda m_0}(\frac{4}{3}Pr_g - 1) & f_1 < \zeta < 0 \\ P_0(0^+) & \zeta > 0. \end{cases} \quad (5.33)$$

In order that the pyrolysis law (5.21) be satisfied, the temperature at any point along the interface must be identical to the surface temperature σ_p for steady, planar combustion. The expression for θ_0 given by Eq. (5.29) then determines the position of the propellant interface relative to the gas-phase reaction zone as

$$f_1 = m_0 \frac{\lambda}{c} \ln \left\{ \frac{\sigma_p - 1 + \alpha\beta}{\alpha\beta} \right\}. \quad (5.34)$$

The asymptotic behavior of the inner solutions (5.27) - (5.33) for $\zeta \rightarrow \pm\infty$ yields conditions relating the leading-order outer variables in Eq. (5.1) across the surface $z = 0$, which we summarize as

$$[W_0] = M_0^{-1}(\rho_\infty^{-1} - 1) \quad (5.35)$$

$$[V_0 + W_0 \nabla\Phi_{r,0}] = 0 \quad (5.36)$$

$$[P_0] = -(\rho_\infty^{-1} - 1) \quad (5.37)$$

$$M_0^{-1} \equiv \left\{ W_0 - V_0 \cdot \nabla\Phi_{r,0} - \frac{\partial\Phi_{r,0}}{\partial t} \right\}_{z=0^-} = (1 + |\nabla\Phi_{r,0}|^2)^{1/2}. \quad (5.38)$$

In addition, the temperature and density fields are fully determined on either side of $z = 0$ as

$$T_0 = \begin{cases} \sigma & z < 0 \\ 1 & z > 0 \end{cases} \quad (5.39)$$

$$R_0 = \begin{cases} 1 & z < 0 \\ \rho_\infty & z > 0, \end{cases} \quad (5.40)$$

which implies that to leading order in δ the burned gas is incompressible. These leading order results (5.35)-(5.38) are identical to those prescribed by Landau (1944) in his treatment of a gas flame as a surface of density discontinuity. We also remark that our results are valid for both liquid and solid propellant combustion. However, when investigating the case of the solid propellant, the velocity field in the solid-phase must be taken to be zero. In that case, Eqs. (5.35)-(5.37) are then interpreted as boundary conditions for $W_0(0^+)$, $\mathbf{V}_0(0^+)$ and $P_0(0^+)$, and the flame speed equation (5.38) reduces to

$$M_0^- = -\frac{\partial \Phi_{r,0}}{\partial t} = (1 + |\nabla \Phi_{r,0}|^2)^{1/2}. \quad (5.41)$$

Since the flow field on either side of $z = 0$ is incompressible to leading order, the problem has been reduced to solving the fluid-dynamic equations in the gas phase,

$$\frac{\partial M_0}{\partial z} + \rho_\infty \nabla \cdot \mathbf{V}_0 = 0 \quad (5.42)$$

$$\rho_\infty \frac{\partial \mathbf{V}_0}{\partial t} + M_0 \frac{\partial \mathbf{V}_0}{\partial z} + \rho_\infty \mathbf{V}_0 \cdot \nabla \mathbf{V}_0 = -\nabla P_0 + \nabla \Phi_{r,0} \frac{\partial P_0}{\partial z} \quad (5.43)$$

$$\rho_\infty \frac{\partial W_0}{\partial t} + M_0 \frac{\partial W_0}{\partial z} + \rho_\infty \mathbf{V}_0 \cdot \nabla W_0 = -\frac{\partial P_0}{\partial z}, \quad (5.44)$$

and in either the liquid phase (for liquid propellants),

$$\frac{\partial M_0}{\partial z} + \nabla \cdot \mathbf{V}_0 = 0 \quad (5.45)$$

$$\frac{\partial \mathbf{V}_0}{\partial t} + M_0 \frac{\partial \mathbf{V}_0}{\partial z} + \mathbf{V}_0 \cdot \nabla \mathbf{V}_0 = -\nabla P_0 + \nabla \Phi_{r,0} \frac{\partial P_0}{\partial z} \quad (5.46)$$

$$\frac{\partial W_0}{\partial t} + M_0 \frac{\partial W_0}{\partial z} + \mathbf{V}_0 \cdot \nabla W_0 = -\frac{\partial P_0}{\partial z}, \quad (5.47)$$

or the solid phase (for solid propellants),

$$W_0 = \mathbf{V}_0 \equiv 0, \quad (5.48)$$

subject to the conditions (5.35)-(5.38). The steady, one-dimensional solution of this system is given by

$$\Phi_{r,0}^* = -t \quad (5.49)$$

$$W_0^* = \begin{cases} 0 & z < 0 \\ \rho_\infty^{-1} - 1 & z > 0 \end{cases} \quad (5.50)$$

$$P_0^* = \begin{cases} \rho_\infty^{-1} - 1 & z < 0 \\ 0 & z > 0 \end{cases} \quad (5.51)$$

$$f_1^* = \frac{\lambda}{c} \ln \left\{ \frac{\sigma_p - 1 + \alpha\beta}{\alpha\beta} \right\}. \quad (5.52)$$

This solution, which can also be obtained easily from Eqs. (4.1), (4.5)-(4.7) by setting $z_0^0 = \delta f_1^*$ and letting $\delta \rightarrow 0$, represents a steady, planar mode of combustion.

§6. Linear Stability Analysis

In order to determine the response of steady, planar burning to small disturbances, we introduce the spatially periodic perturbations

$$\begin{aligned}
 \Phi_r &= \Phi_r^* + \exp(\omega t + ik_1 x + ik_2 y) \\
 w &= W^* + W'(z) \exp(\omega t + ik_1 x + ik_2 y) \\
 \mathbf{v} &= \mathbf{V}^* + \mathbf{V}'(z) \exp(\omega t + ik_1 x + ik_2 y) \\
 p &= P^* + P'(z) \exp(\omega t + ik_1 x + ik_2 y)
 \end{aligned} \tag{6.1}$$

where ω is the growth rate whose sign will determine stability, and primes are used to denote perturbed variables. Here the dimensionless wavenumbers are given by $k_1 = \tilde{k}_1/K$, $k_2 = \tilde{k}_2/K$ where $K = \sqrt{\tilde{k}_1^2 + \tilde{k}_2^2}$. This introduces the hydrodynamic length scale $L = K^{-1}$ which was used to nondimensionalize distances in Section 2. The expansions (6.1) are inserted into the governing equations, which to leading order are given by Eqs. (5.35) - (5.38), (5.42) - (5.47), and nonlinear terms are neglected. This results in a system of linear equations for the perturbed variables and the growth rate, for which solutions are sought as power series in δ (e.g., $\omega \sim \omega_0 + \delta\omega_1 + \dots$).

§6.1. Leading Order Linear Stability of Liquid Propellants

For liquid propellants, the leading order linear stability analysis is identical to that for a gas flame, and indeed we obtain Landau's (1944) result for the growth rate ω_0 , i.e.,

$$\omega_0 = \frac{1}{\rho_\infty + 1} \left\{ -1 + \sqrt{1 - \rho_\infty + \rho_\infty^{-1}} \right\}. \tag{6.2}$$

Thus, we conclude that a deflagration propagating through a liquid propellant is unstable due to the density change across the flame. This hydrodynamic instability is suppressed only as $\rho_\infty \rightarrow 1$, a limit that can in fact be approached at high pressures. In addition, it is known that the result (6.2) can be modified by incorporating additional stabilizing effects into the model, such as gravity (Landau, 1944; Levich, 1956), or a phenomenological dependence of the burning rate on the curvature of the flame front (Markstein, 1951, 1964). Also, as has been done for gaseous combustion (cf. Pelcé and Clavin, 1982; Matalon and Matkowsky, 1982), one can study the influence of other parameters on stability by reconsidering the multiphase flame structure and including the $O(\delta)$ terms in our analysis. In this way, one can obtain corrections to the conditions (5.35)-(5.38) which contain effects due to viscosity, surface tension, diffusion, chemical reaction, and pyrolysis. While these higher-order terms are regarded in the context of the present analysis as perturbations too small in magnitude to suppress the leading-order hydrodynamic instability, they at least suggest how these additional contributions to the multiphase flame structure can affect this instability.

Before continuing with this investigation, however, we first address the question of stability for the case of solid propellants.

§6.2. Linear Stability of Solid Propellants

Proceeding as before, we linearize our system (5.35) - (5.37), (5.42) - (5.44) about the basic state (5.49) - (5.52). It is clear from Eq. (5.41) that the linearization will result in only the trivial solution for the perturbed variables. Therefore, perturbations can be at most $O(\delta)$ and the leading-order solution is given exactly by (5.49)-(5.52). Thus, it appears that the solid propellant offers more resistance to deformations than does the liquid propellant. Perturbations of this magnitude were also considered by Kaper et.al. (1985), in which case a rigid, planar flameholder was situated within the flame structure. As in that study, in order to determine the leading-order growth rate ω_0 of the disturbance, we must obtain the $O(\delta)$ jump conditions for the outer variables. Hence, we continue our analysis of the inner structure for the $O(\delta)$ variables in the expansions (5.3). In particular, these quantities must satisfy the equations

$$\rho_0 \theta_1 = -\rho_1 \theta_0 \quad (6.3)$$

$$\frac{\partial m_1}{\partial \zeta} = 0 \quad (6.4)$$

$$\frac{\partial \theta_1}{\partial \zeta} - \frac{\lambda}{c} \frac{\partial^2 \theta_1}{\partial \zeta^2} = -m_1 \frac{\partial \theta_0}{\partial \zeta} \quad (6.5)$$

$$\frac{\partial Y_1}{\partial \zeta} - \frac{\lambda}{Le c} \frac{\partial^2 Y_1}{\partial \zeta^2} = -m_1 \frac{\partial Y_0}{\partial \zeta} \quad (6.6)$$

$$\frac{\partial w_1}{\partial \zeta} - \frac{4\lambda}{3c} Pr_g \frac{\partial^2 w_1}{\partial \zeta^2} = -\frac{\partial p_1}{\partial \zeta} - m_1 \frac{\partial w_0}{\partial \zeta} \quad (6.7)$$

$$\frac{\partial \mathbf{v}_1}{\partial \zeta} - \frac{\lambda}{c} Pr_g \frac{\partial^2 \mathbf{v}_1}{\partial \zeta^2} = \nabla \Phi_{r,1} \left(\frac{\partial p_0}{\partial \zeta} - \frac{\lambda}{3c} Pr_g \frac{\partial^2 w_0}{\partial \zeta^2} \right), \quad (6.8)$$

where $\lambda = c = 1$ and $Y_1 = \mathbf{v}_1 = w_1 = 0$ for $\zeta < f_1$, and

$$m_1 = m_{p,1} \equiv \rho_0 \left(w_1 - \frac{\partial \Phi_{r,1}}{\partial t} \right) + \rho_1 (w_0 - 1). \quad (6.9)$$

In addition, the jump conditions at $\zeta = 0$ are given by

$$[\theta_1] = [Y_1] = [w_1] = [\mathbf{V}_1] = 0 \quad (6.10)$$

$$\left[\frac{\partial \theta_1}{\partial \zeta} \right] = -\frac{\beta}{Le} \left[\frac{\partial Y_1}{\partial \zeta} \right] \quad (6.11)$$

$$\left[\frac{\partial \theta_1}{\partial \zeta} \right] = -\alpha \beta c \lambda^{-1} \frac{N}{2} \theta_1(0^+) \quad (6.12)$$

$$\left[\frac{\partial \mathbf{v}_1}{\partial \zeta} + \nabla \Phi_{r,1} \frac{\partial w_0}{\partial \zeta} \right] = 0 \quad (6.13)$$

$$[p_1] = \frac{4}{3} Pr_g \frac{\lambda}{c} \left[\frac{\partial w_1}{\partial \zeta} \right], \quad (6.14)$$

and the boundary conditions at $\zeta = f_1$ are

$$[\theta_1] = - \left[\frac{\partial \theta_0}{\partial \zeta} \right] f_2 \quad (6.15)$$

$$m_{p,1} |_{\zeta=f_1} = - \frac{\partial \Phi_{r,1}}{\partial t} = \frac{N_p}{\sigma_p} \left(\frac{\partial \theta_0}{\partial \zeta} f_2 + \theta_1 \right)^+ \quad (6.16)$$

$$\left\{ (c-1)\theta_0^+ + \sigma - c(1-\alpha\beta) \right\} m_{p,1} |_{\zeta=f_1} = \left(\lambda \frac{\partial \theta_1^+}{\partial \zeta} - \frac{\partial \theta_1^-}{\partial \zeta} \right) + \theta_1^- - c\theta_1^+ \quad (6.17)$$

$$(Y_0^+ - \alpha) m_{p,1} |_{\zeta=f_1} = \frac{\lambda}{c Le} \frac{\partial Y_1^+}{\partial \zeta} - Y_1^+ \quad (6.18)$$

$$\mathbf{v}_1 + w_0 \nabla \Phi_{r,1} = 0. \quad (6.19)$$

The problem for the transport variables Y_1 and θ_1 is seen to decouple from the problem for the remaining variables. By applying the conditions (6.10) and (6.18), Y_1 is completely determined as

$$Y_1 = \begin{cases} 0 & \zeta < f_1 \\ -\frac{\alpha c Le}{\lambda} m_1 \zeta \exp\left(\frac{Le \zeta}{\lambda}\right) & f_1 < \zeta < 0 \\ 0 & \zeta > 0. \end{cases}, \quad (6.20)$$

and θ_1 is given by

$$\theta_1 = \begin{cases} \frac{2}{N} m_1 c + m_1 \zeta (\sigma_p - \sigma) \exp(\zeta - f_1) + B \exp(\zeta) & \zeta < f_1 \\ -\frac{\alpha \beta c}{\lambda} m_1 \zeta \exp\left(\frac{\zeta}{\lambda}\right) + \frac{2}{N} m_1 & f_1 < \zeta < 0 \\ \frac{2}{N} m_1 & \zeta > 0, \end{cases} \quad (6.21)$$

where

$$B = m_1 \left\{ \frac{2}{N} (1-c) \right\} + (m_1 + f_2) \left[\frac{\alpha \beta c}{\lambda} \exp(c f_1 / \lambda) - \sigma_p + \sigma \right], \quad (6.22)$$

and f_2 is determined completely by the pyrolysis law (6.16). We observe that θ_1 does not decay to zero as $\zeta \rightarrow -\infty$. Consequently, it is necessary to consider a far-field expansion in order to describe the decay of the $O(\delta)$ temperature perturbation to zero. However, since the far-field behavior does not affect the growth rate ω_0 , we do not pursue this point further. Solutions for the velocity field are now readily obtained, and by matching to $\zeta \rightarrow \infty$ we obtain the following boundary conditions for the outer variables

$$W_1(0^+) = \frac{\partial \Phi_{r,1}}{\partial t} \{1 - \rho_\infty^{-1} (1 + 2/N)\} \quad (6.23)$$

$$\mathbf{V}_1(0^+) = -\nabla \Phi_{r,1} (\rho_\infty^{-1} - 1) \quad (6.24)$$

$$P_1(0^+) = -2 \frac{\partial \Phi_{r,1}}{\partial t} \{1 - \rho_\infty^{-1} (1 + 1/N)\}. \quad (6.25)$$

Finally, in contrast to the gas flame problem (Matalon and Matkowsky, 1982), temperature and density variations in the burned gas cannot be discarded as higher order effects, and the compressibility of the burned gasses must be taken into account. Hence, when solving for the outer variables (5.1) at $O(\delta)$, we must consider the coupling of the equation for T_1 to the hydrodynamic equations. Thus, in addition to Eqns. (6.23) - (6.25), a boundary condition for T_1^+ is needed which is given by the asymptotic behavior of the inner solution (6.21) as $\zeta \rightarrow \infty$, namely

$$T_1(0^+) = -\frac{2}{N} \frac{\partial \Phi_{r,1}}{\partial t}. \quad (6.26)$$

The governing equations in the gas phase for the $O(\delta)$ variables in (5.1) are given by

$$\frac{\partial M_1}{\partial z} + \rho_\infty \nabla \cdot \mathbf{V}_1 + \frac{\partial R_1}{\partial t} = 0 \quad (6.27)$$

$$\rho_\infty \frac{\partial T_1}{\partial t} + \frac{\partial T_1}{\partial z} = 0 \quad (6.28)$$

$$R_1 = -\rho_\infty T_1 \quad (6.29)$$

$$\rho_\infty \frac{\partial \mathbf{V}_1}{\partial t} + \frac{\partial \mathbf{V}_1}{\partial z} = -\nabla P_1 \quad (6.30)$$

$$\rho_\infty \frac{\partial W_1}{\partial t} + \frac{\partial W_1}{\partial z} = -\frac{\partial P_1}{\partial z}, \quad (6.31)$$

where

$$M_1 = \rho_\infty \left(W_1 - \frac{\partial \Phi_{r,1}}{\partial t} \right) + R_1 (W_0 + 1), \quad (6.32)$$

and the steady, planar solution of these equations which satisfies the boundary conditions (6.23) - (6.26) is the trivial one. The linear stability analysis at this order is straightforward and the growth rate ω_0 is found to satisfy the dispersion relation

$$\rho_\infty \omega_0^2 (1 - \nu) + \omega_0 (2 - \nu) + 1 = 0, \quad (6.33)$$

where ν is given by

$$\nu = 2/[N(\rho_\infty - 1)]. \quad (6.34)$$

Both roots of Eq. (6.33) are seen to be negative for $\rho_\infty < 1$ and all values of the activation energy N . Consequently, despite the existence of a deformable interface of density discontinuity, we conclude that the planar combustion front is absolutely stable to hydrodynamic disturbances. Thus, for the case of the solid propellant, a perturbed flow field in the gas phase is not sufficient to render the deflagration unstable. For a liquid propellant, however, hydrodynamic perturbations can exist in the liquid as well as the gas phases, and thus, as we have seen, Landau instability is not suppressed. We note that this result is obtained though the use of a long-wave theory, and so non-acoustic instabilities observed during solid propellant combustion (*cf.* Hightower and Price, 1967) must be attributed to other types of (short-wave) disturbances, such as the reactive-diffusive instabilities that occur on the diffusional length scale l_D (Margolis and Williams, 1988, 1989).

§7. Effects of Flame Structure on Liquid Propellant Stability

We now return to the liquid propellant problem and obtain the $O(\delta)$ correction (ω_1) to the growth rate (6.2). Thus, we now consider the next order flame structure problem, the details of which are contained in the Appendix. As was the case for the solid propellant, the burned gas is compressible and the hydrodynamic equations do not decouple from the thermal transport equation. Thus when deriving corrections to the jump conditions (5.35)-(5.38) we will also obtain a condition on T_1 . We summarize these results as

$$\begin{aligned}
 W_1(0^+) &= \frac{\partial \Phi_{r,1}}{\partial t} + \rho_\infty^{-1}(A_1 + A_5) \\
 W_1(0^-) &= \frac{\partial \Phi_{r,1}}{\partial t} + A_2 \\
 [\mathbf{V}_1] &= -\nabla \Phi_{r,1} [W_1] + \mathbf{A}_3 \\
 [P_1] &= -[W_1] + A_4 - \frac{\lambda}{c}(Pr_g - Pr_l) \{ \nabla \cdot \mathbf{V}_0(0^+) + \nabla^2 \Phi_{r,0} W_0(0^+) \} \\
 T_1(0^+) &= A_5
 \end{aligned} \tag{7.1}$$

where the A_i 's, which are given in the Appendix, depend on the various physical parameters in the problem. An expression for the correction f_2 to the distance between the propellant surface and the reaction zone is found in terms of $\Phi_{r,1}$ by applying the pyrolysis law. Thus the separation distance is fully determined by the structure analysis and neither f_2 nor the pyrolysis activation energy N_p will play a role in the solution of the outer problem.

The only steady, planar solution at this order is the trivial one, and so our entire basic state is comprised of the leading order expressions (5.49)-(5.52) together with (5.39) -(5.40). In order to carry out the linear stability analysis at this order we must, in addition to introducing the perturbations to the hydrodynamic field (6.1), also allow for perturbations to the temperature and density as

$$\begin{aligned}
 T &= T^* + T'(z) \exp(\omega t + ik_1 x + ik_2 y), \quad T' \sim \delta T'_1 + \dots \\
 \rho &= R^* + R'(z) \exp(\omega t + ik_1 x + ik_2 y), \quad R' \sim \delta R'_1 + \dots
 \end{aligned} \tag{7.2}$$

Thus, we obtain the system of linearized equations

$$R'_1 = -\rho_\infty T'_1 \tag{7.3}$$

$$\rho_\infty \omega_0 T'_1 + \frac{dT'_1}{dz} = 0 \tag{7.4}$$

$$M'_1 = \rho_\infty (w'_1 - \omega_1) + R'_1 (W_0^* + 1) \tag{7.5}$$

$$\omega_0 R'_1 + \rho_\infty ik_1 u'_1 + \rho_\infty ik_2 v'_1 + \frac{dM'_1}{dz} = 0 \tag{7.6}$$

$$\rho_\infty \omega_0 w'_1 + \frac{dw'_1}{dz} = \rho_\infty \omega_1 w'_0 - \frac{dp'_1}{dz} + Pr_g \frac{\lambda}{c} \left(\frac{d^2}{dz^2} - 1 \right) w'_0 \tag{7.7}$$

$$\rho_\infty \omega_0 u'_1 + \frac{du'_1}{dz} = \rho_\infty \omega_1 u'_0 - ik_1 p'_1 + Pr_g \frac{\lambda}{c} \left(\frac{d^2}{dz^2} - 1 \right) u'_0 \tag{7.8}$$

$$\rho_\infty \omega_0 v_1' + \frac{dv_1'}{dz} = \rho_\infty \omega_1 v_0' - ik_2 p_1' + Pr_g \frac{\lambda}{c} \left(\frac{d^2}{dz^2} - 1 \right) v_0' \quad (7.9)$$

for $z > 0$, and

$$R_1' = 0 \quad (7.10)$$

$$\rho_\infty \omega_0 T_1' + \frac{dT_1'}{dz} = 0 \quad (7.11)$$

$$M_1' = w_1' - \omega_1 \quad (7.12)$$

$$\frac{dw_1'}{dz} + ik_1 u_1' + ik_2 v_1' = 0, \quad (7.13)$$

and Eqs. (7.7) - (7.9) with $\rho_\infty = 1$ and Pr_g replaced by Pr_l , for $z < 0$. Upon solving these equations subject to the appropriate linearized form of the jump conditions (7.1) we obtain a solvability condition for ω_1 as

$$\begin{aligned} 2[\omega_0(\rho_\infty + 1) + 1]\omega_1 = & -\gamma - 2Pr_g \frac{\lambda}{c} \left(\frac{\sigma_p}{\rho_\infty} - 1 \right) + \frac{\lambda \ln \sigma_p}{c(1 - \alpha\beta)} \left\{ \omega_0^2 - 1 - \rho_\infty^{-1} \right. \\ & + (N + 1)(\rho_\infty \omega_0 + 1)(\omega_0 + 1) \left. \right\} + \frac{\lambda}{c} \rho_\infty^{-1} (\sigma_p - 1) \\ & - (\omega_0 + \rho_\infty^{-1})(\omega_0 + 1) \left\{ (N + 1)(\sigma_p - \sigma)/c + \frac{\rho_\infty}{1 - \alpha\beta} [-Le I_1 \right. \\ & + \frac{\lambda}{c} (1 - \exp(c Le f_1/\lambda)) (\ln \sigma_p - Le^{-1}) \left. \right] [\alpha\beta(N + 1) - 2] \left. \right\} \\ & + f_1 \left\{ (\omega_0 + 1) \left(-1 + \frac{\rho_\infty}{1 - \alpha\beta} \right) \rho_\infty^{-1} (-2\rho_\infty \omega_0 - 1 - \omega_0) \right. \\ & \left. - (\rho_\infty^{-1} - 1)^2 + \frac{\alpha^2 \beta^2}{\rho_\infty(1 - \alpha\beta)} \right\}, \quad (7.14) \end{aligned}$$

where

$$I_1 = \int_{f_1}^0 e^{c Le \zeta/\lambda} \ln(1 - \alpha\beta + \alpha\beta e^{c\zeta/\lambda}) d\zeta. \quad (7.15)$$

The expression (7.14) reveals a dependence on all the physical parameters in the problem (*i.e.*, ρ_∞ , Pr_g , Le , γ , $\alpha\beta$, λ , c), suggesting that each plays a comparable role in determining the stability of liquid propellant combustion. It is easily seen that surface tension and viscous effects are always stabilizing for this problem. Also, we observe that while ω_1 depends on Pr_g , it is independent of Pr_l , suggesting that the gas phase viscosity has a larger influence on hydrodynamic stability than the viscosity of the liquid propellant. In addition, we note that the coefficient multiplying Pr_g is proportional to the density jump across the propellant surface. If this jump is eliminated (*i.e.*, if $\rho_\infty/\sigma_p = 1$), then ω_1 becomes independent of Pr_g and viscosity becomes a secondary effect, just as in the case of a freely propagating gas flame (cf. Frankel and Sivashinsky, 1982, Matalon and Matkowsky, 1982). In fact, if the gas-phase reaction zone is far away from the propellant surface (*i.e.*, $f_1 \rightarrow -\infty$), then by setting $\sigma_p = \sigma = \rho_\infty$, $\lambda = c = 1$, $Le = 1 + l/N$, and letting $N \rightarrow \infty$, Eq. (7.14) reduces to

$$\omega_1 = \frac{(\rho_\infty^{-1} - 1) + (\rho_\infty - 1)^{-1} [2\omega_0 + (1 + \rho_\infty^{-1})] \ln \rho_\infty - l l \rho_\infty (\omega_0 + 1) [\omega_0 + 1/\rho_\infty]}{2[\omega_0(1 + \rho_\infty) + 1]}, \quad (7.16)$$

where

$$I = \int_{-\infty}^0 \ln[1 + (\rho_{\infty}^{-1} - 1) \exp(x)] dx, \quad (7.17)$$

and the gas flame result is recovered.

The dependence of ω_1 on Le , $\alpha\beta$, and N is more complex and will now be investigated. In what follows, we will simplify matters by setting $\gamma = Pr_g = 0$ (since these effects have already been shown to be stabilizing) and $\lambda = c = 1$. First, in the intrusive limit that $f_1 \rightarrow 0$ (i.e., $\sigma_p \rightarrow 1$), Eq. (7.14) collapses to

$$\omega_1 = \frac{-(\omega_0 + 1)(\omega_0 + 1/\rho_{\infty})(N + 1)(1 - \sigma)}{2[\omega_0(1 + \rho_{\infty}) + 1]} < 0. \quad (7.18)$$

This expression, since it is always negative, indicates a tendency to stabilize the flame, independent of the Lewis number. This feature can be seen in Figs. 2 and 3, in which ω_1 is plotted as a function of f_1 according to (7.14) for various values of the Lewis number. Also illustrated in these figures is the sensitivity of the growth rate correction to Le for nonzero values of the distance $-f_1$ between the propellant surface and the gas-phase reaction front. In particular, as in the case of freely propagating flames, an increase in Lewis number is seen to have a stabilizing influence on the leading-order hydrodynamic (cellular) instability. As $-f_1$ becomes large, the curves in Fig. 2 asymptote to a constant value. In that figure, we have chosen $\rho_{\infty} = 1 - \alpha\beta$ so that as $N \rightarrow \infty$ with $N(Le - 1) \rightarrow l \sim O(1)$, these curves approach the gas flame result (7.16) for large $-f_1$. In Fig. 3, we have chosen $\rho_{\infty} < 1 - \alpha\beta$ to insure that the liquid is more dense than the gas even in the limit that the separation distance is large ($f_1 \rightarrow -\infty$, $\sigma_p \rightarrow 1 - \alpha\beta$). We note that the slope of $\omega_1(-f_1)$ is negative in that limit, which implies a tendency toward stabilization for $-f_1$ sufficiently large.

In order to determine how the gas-phase activation energy modifies the behavior of ω_1 , Fig. 4 was plotted with the same parameter values as Fig. 2 with the exception of N , which was decreased from 100 to 50. From Eq. (7.18) we expect the correction ω_1 to the growth rate to be proportional to the value of N in the intrusive limit that $f_1 \rightarrow 0$. Indeed, by comparing these figures, this is observed to be the case, and in particular, an increase in N is seen to have a stabilizing effect. For nonzero f_1 , the curves in each figure exhibit the same qualitative behavior, and as the separation distance $-f_1$ is increased, the effect of the gas-phase activation energy becomes less significant, especially for values of Le near unity. As N is increased, then (as in the case of freely propagating flames) ω_1 is seen to decrease (increase) for larger values of $-f_1$ if the thermal diffusivity of the gas is greater (less) than the mass diffusivity [i.e., $Le > (<) 1$].

We now consider the effect of ρ_{∞} and $\alpha\beta$ on ω_1 . As pointed out earlier, the leading-order hydrodynamic instability is only suppressed in the limit that $\rho_{\infty} \rightarrow 1$, in which case the liquid does not expand upon pyrolyzing and/or vaporizing at the propellant surface. To be consistent, when considering this limit we must simultaneously consider the limit $\sigma_p \rightarrow 1$, which can occur either as $f_1 \rightarrow 0$ or as $\alpha\beta \rightarrow 0$. The former (intrusive) limit was explored earlier, resulting in the simplified expression (7.18) for ω_1 , which exhibits no dependence on pyrolysis. This expression is reduced

further by setting $\rho_\infty = 1$ and $\omega_0 = 0$ to give

$$\omega_1 = \frac{1}{2}(N+1)(\sigma-1). \quad (7.19)$$

In the alternative limit that $\alpha\beta$ approaches 0, most of the propellant is pyrolyzed directly into gaseous products, leaving only a vanishingly small fraction to burn in the gas phase. By concurrently taking the limits $\rho_\infty \rightarrow 1$ and $\alpha\beta \rightarrow 0$, Eq. (7.14) reduces to

$$\omega_1 = \frac{1}{2}(N+1)(\sigma-1) - Le^{-1} (1 - e^{Le f_1}) < 0. \quad (7.20)$$

Thus, as the reaction zone moves further away from the pyrolyzing interface, an increase in Lewis number results in increased values of ω_1 . This trend is observed by comparing Figs. 5 and 6 in which plots were made with ρ_∞ near unity and $\alpha\beta \ll 1$ for two different values of Lewis number. Also illustrated in these figures is the dependence of the growth rate correction on density change and fraction of vaporization. In particular, ω_1 is seen to increase with either ρ_∞ or $\alpha\beta$.

In Figs. 7 and 8, plots were made for the same two values of Lewis number ($Le = .8, 1.3$) used in Figs. 5 and 6, respectively, but ρ_∞ and $\alpha\beta$ were taken to be nearly equal to one another. In these graphs, ω_1 is seen to increase with ρ_∞ and $\alpha\beta$ in the same way as before, but here an increase in Le is accompanied by a decrease in ω_1 . Finally, the curves in Figs. 9 and 10 were generated for the case in which $\rho_\infty \ll 1$ and $\alpha\beta \approx 1$. As the separation distance $-f_1$ is increased from 0, where it follows from Eq. (7.18) that $\omega_1 = O(\rho_\infty^{-1})$, the curves become extremely sensitive to the values of ρ_∞ , $\alpha\beta$, and Le . In particular, we observe that an increase in Le or a decrease in either ρ_∞ or $\alpha\beta$ can result in negative values of ω_1 , thus implying that the multiphase flame structure has a stabilizing effect on the leading-order hydrodynamic instability.

§8. Summary

The present work has considered the hydrodynamic stability of solid and liquid propellant combustion. Under the assumption that the thickness of the multiphase flame structure is small compared to the characteristic length scale of a hydrodynamic disturbance, the method of matched asymptotic expansions was used to derive jump conditions on the outer fluid and temperature variables across this structure. Our results for the case of a solid propellant differ radically from those for a freely propagating gas flame, for it is shown that the absence of fluid perturbations in the solid phase completely suppresses Landau instability. Thus, it appears that the only type of non-acoustic instability that is possible for this problem is reactive/diffusive in nature, in which either pulsating or cellular perturbations to steady, planar burning occur on diffusive, rather than hydrodynamic, length and time scales (Margolis and Armstrong, 1986; Margolis and Williams, 1988, 1989).

For the liquid propellant, however, perturbations of the fluid variables in the liquid phase must be taken into account, and to leading order, Landau's (1944) result is recovered. However, the leading order growth rate can become small when the ratio ρ_∞ of the burned gas density to that of the liquid propellant is close to unity, a regime which can be achieved at very high pressures. Consequently, it has been shown that the next-order correction to the growth rate can be stabilizing, and in an appropriate limiting case which includes a large separation distance between the propellant surface and the gas-phase reaction zone, the results corresponding to a freely propagating gas flame (*cf.* Matalon and Matkowsky, 1982) are recovered. More generally, however, it was determined that this separation distance, along with other parameters in the problem, can significantly influence both the sign and the magnitude of the growth rate. For example, for small values of the separation distance, it was found that the liquid propellant is more likely to experience hydrodynamic instability than the freely propagating gas flame when the density ratio ρ_∞ is close to unity and most of the reaction occurs through pyrolysis at the propellant surface (*cf.* Figs. 5-6), whereas the opposite is true when ρ_∞ is smaller and a more significant fraction of the propellant vaporizes and burns in the gas phase (*cf.* Figs. 7-8).

Appendix

When considering the $O(\delta)$ flame structure problem, we must solve an inhomogeneous system of equations of the form shown in Eqs. (5.4) - (5.26). At this order, the equations in the gas phase are

$$\rho_1 \theta_0 = -\rho_0 \theta_1 \quad (\text{A.21})$$

$$\frac{\partial m_1}{\partial \zeta} = -\frac{\partial \rho_0}{\partial t} - \nabla \cdot (\rho_0 \mathbf{v}_0) \quad (\text{A.22})$$

$$\begin{aligned} m_0 \frac{\partial \theta_1}{\partial \zeta} - \frac{\lambda}{c} m_0^2 \frac{\partial^2 \theta_1}{\partial \zeta^2} &= -m_1 \frac{\partial \theta_0}{\partial \zeta} - \rho_0 \left(\frac{\partial \theta_0}{\partial t} + \mathbf{v}_0 \cdot \nabla \theta_0 \right) + \frac{\lambda}{c} \left\{ 2 \nabla \Phi_{r,0} \cdot \Phi_{r,1} \frac{\partial^2 \theta_0}{\partial \zeta^2} \right. \\ &\quad \left. - \nabla^2 \Phi_{r,0} \frac{\partial \theta_0}{\partial \zeta} - 2 \nabla \Phi_{r,0} \cdot \nabla \frac{\partial \theta_0}{\partial \zeta} \right\} \end{aligned} \quad (\text{A.23})$$

$$\begin{aligned} m_0 \frac{\partial Y_1}{\partial \zeta} - \frac{\lambda}{c Le} m_0^2 \frac{\partial^2 Y_1}{\partial \zeta^2} &= -m_1 \frac{\partial Y_0}{\partial \zeta} - \rho_0 \left(\frac{\partial Y_0}{\partial t} + \mathbf{v}_0 \cdot \nabla Y_0 \right) + \frac{\lambda}{c Le} \left\{ 2 \nabla \Phi_{r,0} \cdot \Phi_{r,1} \frac{\partial^2 Y_0}{\partial \zeta^2} \right. \\ &\quad \left. - \nabla^2 \Phi_{r,0} \frac{\partial Y_0}{\partial \zeta} - 2 \nabla \Phi_{r,0} \cdot \nabla \frac{\partial Y_0}{\partial \zeta} \right\}, \quad Y_0 \equiv 0 \text{ for } \zeta > 0 \end{aligned} \quad (\text{A.24})$$

$$m_0 \frac{\partial w_1}{\partial \zeta} - \frac{\lambda}{c} Pr_g \left\{ m_0^2 \frac{\partial^2 w_1}{\partial \zeta^2} + \frac{1}{3} \left(\frac{\partial^2 w_1}{\partial \zeta^2} - \nabla \Phi_{r,0} \cdot \frac{\partial^2 \mathbf{v}_1}{\partial \zeta^2} \right) \right\} + \frac{\partial p_1}{\partial \zeta} = m_1 \frac{\partial w_0}{\partial \zeta}$$

$$\begin{aligned}
& -\rho_0 \left(\frac{\partial w_0}{\partial t} + \mathbf{v}_0 \cdot \nabla w_0 \right) + \frac{\lambda Pr_g}{c} \left\{ 2\nabla \Phi_{r,0} \cdot \Phi_{r,1} \frac{\partial^2 w_0}{\partial \zeta^2} - \nabla^2 \Phi_{r,0} \frac{\partial w_0}{\partial \zeta} \right. \\
& \left. - 2\nabla \Phi_{r,0} \cdot \nabla \frac{\partial w_0}{\partial \zeta} + \frac{1}{3} \left[\nabla \frac{\partial \mathbf{v}_0}{\partial \zeta} - \nabla \Phi_{r,1} \cdot \frac{\partial^2 \mathbf{v}_0}{\partial \zeta^2} \right] \right\} \quad (\text{A.25})
\end{aligned}$$

$$\begin{aligned}
m_0 \left(\frac{\partial \mathbf{v}_1}{\partial \zeta} + \nabla \Phi_{r,0} \frac{\partial w_1}{\partial \zeta} \right) - \frac{\lambda}{c} Pr_g m_0^2 \left(\frac{\partial^2 \mathbf{v}_1}{\partial \zeta^2} + \nabla \Phi_{r,0} \frac{\partial^2 w_1}{\partial \zeta^2} \right) &= -\nabla p_0 + \Phi_{r,1} \frac{\partial p_0}{\partial \zeta} \\
& - \rho_0 \left\{ \frac{\partial \mathbf{v}_0}{\partial t} + \mathbf{v}_0 \cdot \nabla \mathbf{v}_0 + \Phi_{r,0} \left(\frac{\partial w_0}{\partial t} + \mathbf{v}_0 \cdot \nabla w_0 \right) \right\} + \frac{\lambda Pr_g}{3c} \left[-m_0^2 \nabla \Phi_{r,1} \frac{\partial^2 w_0}{\partial \zeta^2} \right. \\
& \left. + 4 \frac{\partial w_0}{\partial \zeta} m_0 \nabla m_0 + m_0^2 \nabla \left(\frac{\partial w_0}{\partial \zeta} \right) \right], \quad (\text{A.26})
\end{aligned}$$

while in the condensed phase,

$$\rho_1 = Y_1 = 0 \quad (\text{A.27})$$

$$\frac{\partial m_1}{\partial \zeta} = -\nabla \cdot \mathbf{v}_0 \quad (\text{A.28})$$

$$\begin{aligned}
m_0 \frac{\partial \theta_1}{\partial \zeta} - m_0^2 \frac{\partial^2 \theta_1}{\partial \zeta^2} &= -m_1 \frac{\partial \theta_0}{\partial \zeta} - \rho_0 \left(\frac{\partial \theta_0}{\partial t} + \mathbf{v}_0 \cdot \nabla \theta_0 \right) + 2\nabla \Phi_{r,0} \cdot \Phi_{r,1} \frac{\partial^2 \theta_0}{\partial \zeta^2} \\
& - \nabla^2 \Phi_{r,0} \frac{\partial \theta_0}{\partial \zeta} - 2\nabla \Phi_{r,0} \cdot \nabla \frac{\partial \theta_0}{\partial \zeta}, \quad (\text{A.29})
\end{aligned}$$

and Eqs. (A.5) - (A.6) with $\rho_0 = 1$, $\rho_1 = 0$ and Pr_g replaced by Pr_l . In addition, the jump conditions at $\zeta = 0$ are given by

$$[\theta_1] = [Y_1] = [w_1] = [\mathbf{V}_1] = 0, \quad (\text{A.30})$$

$$\left[\frac{\partial \theta_1}{\partial \zeta} \right] = -\frac{\beta}{Le} \left[\frac{\partial Y_1}{\partial \zeta} \right] \quad (\text{A.31})$$

$$\left[\frac{\partial \theta_1}{\partial \zeta} \right] = -\alpha \beta c \lambda^{-1} m_0^{-1} \left\{ \frac{N}{2} \theta_1(0^+) + m_0^{-2} \nabla \Phi_{r,0} \cdot \nabla \Phi_{r,1} \right\}, \quad (\text{A.32})$$

$$\left[\frac{\partial \mathbf{v}_1}{\partial \zeta} + \nabla \Phi_{r,0} \frac{\partial w_1}{\partial \zeta} \right] = \nabla \Phi_{r,1} \left[\frac{\partial w_0}{\partial \zeta} \right], \quad (\text{A.33})$$

$$[p_1] = \frac{4}{3} Pr_g \frac{\lambda}{c} \left(m_0^2 \left[\frac{\partial w_1}{\partial \zeta} \right] + 2\nabla \Phi_{r,0} \cdot \nabla \Phi_{r,1} \left[\frac{\partial w_0}{\partial \zeta} \right] \right), \quad (\text{A.34})$$

and the boundary conditions at the interface $\zeta = f_1$ are

$$[[m_{p,1}]] = 0 \quad (\text{A.35})$$

$$[[\theta_1]] = -[[\frac{\partial \theta_0}{\partial \zeta}]] f_2 \quad (\text{A.36})$$

$$m_{p,1}|_{\zeta=f_1} = m_0 \frac{N_p}{\sigma_P} \left(\frac{\partial \theta_0}{\partial \zeta} f_2 + \theta_1 \right)^+ + m_0^{-1} \nabla \Phi_{r,0} \cdot \nabla \Phi_{p,1} \quad (\text{A.37})$$

$$\begin{aligned} \{(c-1)\theta_0^+ + \sigma - c(1-\alpha\beta)\}m_{p,1}|_{\zeta=f_1} &= m_0^2 \left(\lambda \frac{\partial \theta_1^+}{\partial \zeta} - \frac{\partial \theta_1^-}{\partial \zeta} \right) + m_0(\theta_1^- - c\theta_1^+) \\ &+ (\nabla \Phi_{r,0} \cdot \nabla \Phi_{r,1} + \nabla \Phi_{r,0} \cdot \nabla \Phi_{p,1}) \left(\lambda \frac{\partial \theta_0^+}{\partial \zeta} - \frac{\partial \theta_0^-}{\partial \zeta} \right) - \nabla \Phi_{r,0} \cdot \nabla (\lambda \theta_0^+ - \theta_0^-) \quad (\text{A.38}) \end{aligned}$$

$$\begin{aligned} (Y_0^+ - \alpha) m_{p,1}|_{\zeta=f_1} &= \frac{\lambda m_0^2}{cLe} \frac{\partial Y_1^+}{\partial \zeta} - m_0 Y_1^+ + \frac{\lambda}{cLe} \left\{ (\nabla \Phi_{r,0} \cdot \nabla \Phi_{r,1} + \nabla \Phi_{r,0} \cdot \nabla \Phi_{p,1}) \frac{\partial Y_0^+}{\partial \zeta} \right. \\ &\quad \left. - \nabla \Phi_{r,0} \cdot \nabla Y_0^+ \right\} \quad (\text{A.39}) \end{aligned}$$

$$[\mathbf{v}_1 + w_1 \nabla \Phi_{r,0}] = -\nabla \Phi_{r,1} [w_0], \quad (\text{A.40})$$

$$\begin{aligned} Pr_g \left\{ \frac{\partial \mathbf{v}_1}{\partial \zeta} + \nabla \Phi_{r,0} \frac{\partial w_1}{\partial \zeta} + 2 \nabla \Phi_{p,1} \frac{\partial w_0}{\partial \zeta} - \nabla \Phi_{r,1} \frac{\partial w_0}{\partial \zeta} + m_0^{-2} \nabla w_0 - 2m_0^{-2} \nabla \Phi_{r,0} \nabla \mathbf{v}_0 \right. \\ \left. - m_0^{-2} \nabla \Phi_{r,0} (\nabla \Phi_{r,0} \cdot \nabla w_0) + m_0^{-2} \left(\frac{\partial u_0}{\partial y} + \frac{\partial v_0}{\partial x} \right) \left(\frac{\partial \Phi_{r,0}}{\partial y}; \frac{\partial \Phi_{r,0}}{\partial x} \right) \right\}^+ \\ = Pr_l \left\{ \frac{\partial \mathbf{v}_1}{\partial \zeta} + \nabla \Phi_{r,0} \frac{\partial w_1}{\partial \zeta} + 2 \nabla \Phi_{p,1} \frac{\partial w_0}{\partial \zeta} - \nabla \Phi_{r,1} \frac{\partial w_0}{\partial \zeta} + m_0^{-2} \nabla w_0 \right. \\ \left. - 2m_0^{-2} \nabla \Phi_{r,0} \nabla \mathbf{v}_0 - m_0^{-2} \nabla \Phi_{r,0} (\nabla \Phi_{r,0} \cdot \nabla w_0) \right. \\ \left. + m_0^{-2} \left(\frac{\partial u_0}{\partial y} + \frac{\partial v_0}{\partial x} \right) \left(\frac{\partial \Phi_{r,0}}{\partial y}; \frac{\partial \Phi_{r,0}}{\partial x} \right) \right\}^- \quad (\text{A.41}) \end{aligned}$$

$$\begin{aligned} -[p_0] &= [w_1 - \nabla \Phi_{r,0} \cdot \mathbf{v}_1 - \nabla \Phi_{r,1} \cdot \mathbf{v}_0] m_0^{-1} + m_0^{-2} [w_0 - \nabla \Phi_{r,0} \cdot \mathbf{v}_0] m_{p,1}|_{\zeta=f_1} \\ &- 2m_0^{-3} \nabla \Phi_{p,1} \cdot \nabla \Phi_{r,0} [w_0 - \nabla \Phi_{r,0} \cdot \mathbf{v}_0] - \gamma \nabla \cdot \frac{\nabla \Phi_{r,0}}{m_0} \\ &- \frac{\lambda}{c} Pr_g \left\{ \frac{4}{3} \left(\frac{\partial w_1}{\partial \zeta} - \nabla \Phi_{r,0} \cdot \frac{\partial \mathbf{v}_1}{\partial \zeta} \right) + (4/3 + m_0^{-2}) \nabla \Phi_{r,1} \cdot \nabla \Phi_{r,0} - 2m_0^{-2} \nabla \Phi_{r,0} \cdot \nabla w_0 \right. \\ &\quad \left. - \frac{2}{3} \nabla \cdot \mathbf{v}_0 + 2m_0^{-2} \nabla \Phi_{r,0} \cdot \nabla (\mathbf{v}_0 \cdot \nabla \Phi_{r,0}) - m_0^{-2} \mathbf{v}_0 \cdot \nabla (m_0^2) \right\} \\ &+ \frac{\lambda}{c} Pr_l \left\{ \frac{4}{3} \left(\frac{\partial w_1}{\partial \zeta} - \nabla \Phi_{r,0} \cdot \frac{\partial \mathbf{v}_1}{\partial \zeta} \right) + (4/3 + m_0^{-2}) \nabla \Phi_{r,1} \cdot \nabla \Phi_{r,0} - 2m_0^{-2} \nabla \Phi_{r,0} \cdot \nabla w_0 \right. \\ &\quad \left. - \frac{2}{3} \nabla \cdot \mathbf{v}_0 + 2m_0^{-2} \nabla \Phi_{r,0} \cdot \nabla (\mathbf{v}_0 \cdot \nabla \Phi_{r,0}) - m_0^{-2} \mathbf{v}_0 \cdot \nabla (m_0^2) \right\}. \quad (\text{A.42}) \end{aligned}$$

To solve this system, we first integrate Eqs. (A.2) and (A.8) to obtain an expression for m_1 in each region, after which Eqs. (A.3), (A.4) and (A.9) yield solutions for the transport variables θ_1 and Y_1 . Finally, the remaining equations are solved for the hydrodynamic variables. The asymptotic behavior of these solutions as $\zeta \rightarrow \pm\infty$ is then matched to the outer solutions (5.1) expanded in a Taylor series about $z = 0$. Thus, for example, the matching condition at this order for the velocity field in the z -direction is given by

$$\lim_{\zeta \rightarrow \pm\infty} w_1(\zeta, x, y, t) = W_1(z = 0^\pm) + \zeta \frac{\partial W_0}{\partial z}(z = 0^\pm). \quad (\text{A.43})$$

This matching procedure results in conditions (7.1) and lengthy expressions for the A_i 's. In this study, we only require the linearized forms of these expressions, which are given by

$$A_1 = \frac{N}{2(1-\alpha\beta)} \left\{ \rho_\infty \nabla \cdot \mathbf{V}_0(0^+) + \nabla^2 \Phi_{r,0} \right\} \left\{ -\frac{\lambda}{c} \ln \sigma_p \left[\alpha\beta(e^{c f_1/\lambda} - e^{c L e f_1/\lambda}) + \frac{2}{N} e^{c L e f_1/\lambda} \right] - (1-\alpha\beta) \frac{\sigma_p - \sigma}{\rho_\infty c} + \frac{\lambda}{c} \sigma_p \ln \sigma_p + \left(\alpha\beta - \frac{2}{N} \right) \left[L e I_1 + \frac{\lambda}{c L e} (1 - e^{c L e f_1/\lambda}) \right] \right\} \quad (\text{A.44})$$

$$A_2 = A_1 + (\rho_\infty \nabla \cdot \mathbf{V}_0(0^+) + \nabla^2 \Phi_{r,0}) (1-\alpha\beta)^{-1} \left\{ f_1 \left[\rho_\infty^{-1} (1-\alpha\beta) - 1 \right] + \frac{\lambda}{c} \ln \sigma_p \right\} \quad (\text{A.45})$$

$$\begin{aligned} \mathbf{A}_3 \equiv (A_3^1, A_3^2) &= - \left\{ \rho_\infty \frac{\partial \mathbf{V}_0}{\partial t}(0^+) + \frac{\partial \nabla \Phi_{r,0}}{\partial t} \right\} (1-\alpha\beta)^{-1} \left\{ f_1 \left[\rho_\infty^{-1} (1-\alpha\beta) - 1 \right] + \frac{\lambda}{c} \ln \sigma_p \right\} \\ &+ \frac{\lambda}{c} (Pr_g - Pr_l) [\nabla W_0(0^+) - \nabla P_0(0^+)] - \frac{\lambda}{c} \rho_\infty Pr_g \frac{\partial \mathbf{V}_0}{\partial t}(0^+) \\ &+ \frac{\lambda}{c} Pr_l \left[\frac{\partial \mathbf{V}_0}{\partial t}(0^+) + (\rho_\infty^{-1} - 1) \frac{\partial \nabla \Phi_{r,0}}{\partial t}(0^+) \right] \end{aligned} \quad (\text{A.46})$$

$$\begin{aligned} A_4 &= A_2 (1 - \rho_\infty^{-1}) + \gamma \nabla^2 \Phi_{r,0} + \left\{ \nabla \cdot \mathbf{V}_0(0^+) - \rho_\infty \frac{\partial W_0}{\partial t}(0^+) \right\} \left\{ f_1 \left[\rho_\infty^{-1} - (1-\alpha\beta)^{-1} \right] \right. \\ &\left. + \frac{\lambda}{c} \ln \sigma_p \right\} + \nabla^2 \Phi_{r,0} \left\{ f_1 (\rho_\infty^{-1} - 1)^2 - \frac{f_1 \alpha^2 \beta^2}{\rho_\infty (1-\alpha\beta)} + \frac{\lambda}{c \rho_\infty} \left[1 - \sigma_p + \frac{\ln \sigma_p}{(1-\alpha\beta)} \right] \right\} \end{aligned} \quad (\text{A.47})$$

$$\begin{aligned} A_5 &= 2/N \left\{ e^{c L e f_1/\lambda} \left(A_2 - f_1 \left[\nabla \cdot \mathbf{V}_0(0^+) + (\rho_\infty^{-1} - 1) \nabla^2 \Phi_{r,0} \right] \right) \right. \\ &+ (1 - e^{c L e f_1/\lambda}) \left(A_3 + \frac{\lambda}{c L e} \nabla^2 \Phi_{r,0} \right) + L e I_1 \nabla^2 \Phi_{r,0} \\ &\left. + \frac{L e}{1 - \alpha\beta} \left[\rho_\infty \nabla \cdot \mathbf{V}_0(0^+) + \alpha\beta \nabla^2 \Phi_{r,0} \right] \left[I_1 + \frac{\lambda}{c L e} + e^{c L e f_1/\lambda} \left(f_1 - \frac{\lambda}{c L e} \right) \right] \right\}. \end{aligned} \quad (\text{A.48})$$

REFERENCES

- Armstrong, R. C., and Margolis, S. B. (1989a). Hydrodynamic and reactive/ diffusive instabilities in a dynamic model of liquid propellant combustion. *Twenty-Second Symposium (International) on Combustion*, to appear.
- Armstrong, R. C., and Margolis, S. B. (1989). Hydrodynamic and reactive/ diffusive instabilities in a dynamic model of liquid propellant combustion: II. Inviscid Fluid Motions. *Combust. Flame*, to appear.
- Booty, M. R., Margolis, S. B., and Matkowsky, B. J. (1986). Interaction of pulsating and spinning waves in condensed phase combustion. *SIAM J. Appl. Math.* **46**, 801.
- Buckmaster, J. D., and Ludford, G. S. S. (1983). Lectures on mathematical combustion. *CBMS Regional Conference Series in Applied Mathematics* **43**, SIAM, Philadelphia.
- Chu, B. T., and Parlange, J. Y. (1962). On the stability of laminar flames. *J. de Mechanique* **1**, 293.
- Darrieus, G. (1945). Propagation d'un front de flamme. Presented at *Le Congres de Mecanique Appliquee*, unpublished.
- Eckhaus, W. (1961). Theory of flame front stability. *J. Fluid Mech.* **10**, 80.
- Einbinder, H. (1953). The hydrodynamic stability of flame fronts. *J Chem. Phys.* **21**, 480.
- Frankel, M. L., and Sivashinsky, G. I. (1982). The effect of viscosity on hydrodynamic stability of a plane flame front. *Combust. Sci. Technol.* **29**, 207.
- Hightower, J. D., and Price, E. W. (1967). Combustion of ammonium perchlorate. *Eleventh Symposium (International) on Combustion*, pp. 463-472.
- Istratov, A. G., and Librovich, V. B. (1966). The effect of transport processes on the stability of a plane flame front. *J. Appl. Math. Mech. (PMM)*, **30**, 541.
- Joulin, G., and Sivashinsky, G. I. (1983). On the dynamics of nearly-extinguished non-adiabatic cellular flames. *Combust. Sci. Technol.* **31**, 75.
- Kaper, H. G., Leaf, G. K., Matalon, M., and Matkowsky, B. J. (1985). The stability of plane flames attached to a flameholder. *Combust. Sci. Technol.* **43**, 271.
- Landau, L. D. (1944). On the theory of slow combustion. *Acta Physicichimica URSS* **19**, 77.
- Levich, V. G. (1956). On the stability of the flame front when a liquid is burning slowly. *Dokl. Akad. Nauk SSSR* **109**, 975.

- Margolis, S. B. (1980). Bifurcation phenomena in burner-stabilized premixed flames. *Combust. Sci. Technol.* **22**, 143.
- Margolis, S. B. (1983). An asymptotic theory of condensed two-phase flame propagation. *SIAM J. Appl. Math.* **43**, 351.
- Margolis, S. B. (1985). An asymptotic theory of heterogeneous condensed combustion. *Combust. Sci. Technol.* **43**, 197.
- Margolis, S. B., and Armstrong, R. C. (1986). Two asymptotic models for solid propellant combustion. *Combust. Sci. Technol.* **47**, 1.
- Margolis, S. B., Kaper, H. G., Leaf, G. K., and Matkowsky, B. J. (1985). Bifurcation of pulsating and spinning reaction fronts in condensed two-phase combustion. *Combust. Sci. Technol.* **43**, 127.
- Margolis, S. B., and Matkowsky, B. J. (1983). Nonlinear stability and bifurcation in the transition from laminar to turbulent flame propagation. *Combust. Sci. Technol.* **34**, 45.
- Margolis, S. B., and Sivashinsky, G. I. (1984). Flame propagation in vertical channels: bifurcation to bimodal cellular flames. *SIAM J. Appl. Math.* **44**, 344.
- Margolis, S. B., and Williams, F. A. (1988). Diffusional/thermal coupling and intrinsic instability of solid propellant combustion. *Combust. Sci. Technol.* **59**, 27.
- Margolis, S. B., and Williams, F. A. (1989). Diffusional/thermal instability of a solid propellant flame. *SIAM J. Appl. Math.*, to appear.
- Markstein, G. H. (1951). Experimental and theoretical studies of flame front stability. *J. Aero. Sci.* **18**, 199.
- Markstein, G. H. (1964). *Nonsteady Flame Propagation*. Pergamon Press.
- Matalon, M., and Matkowsky, B. J. (1982). Flames as gasdynamic discontinuities. *J. Fluid Mech.* **124**, 239.
- Matalon, M., and Matkowsky, B. J. (1983). Flames in fluids, their interaction and stability. *Combust. Sci. Technol.* **34**, 295.
- Matalon, M., and Matkowsky, B. J. (1984). On the stability of plane and curved flames. *SIAM J. Appl. Math.* **44**, 327.
- Matkowsky, B. J., and Sivashinsky, G. I. (1978). Propagation of a pulsating reaction front in solid fuel combustion. *SIAM J. Appl. Math.* **35**, 465.
- Matkowsky, B. J., and Sivashinsky, G. I. (1979). An asymptotic derivation of two models in flame theory associated with the constant density approximation. *SIAM J. Appl. Math.* **37**, 686.

Merzhanov, A. G., Filonenko, A. K., and Borovinskaya, I. P. (1973). New phenomena in combustion of condensed systems. *Dokl. Phys. Chem.* **208**, 122.

Pelcé, P., and Clavin, R. (1982). Influence of hydrodynamics and diffusion upon the stability limits of laminar premixed flames. *J. Fluid Mech.* **124**, 219.

Sivashinsky, G. I. (1975). Structure of bunsen flames. *J. Chem. Phys.* **62**, 638.

Sivashinsky, G. I. (1977). Diffusional-thermal theory of cellular flames. *Combust. Sci. Technol.* **15**, 137.

Sivashinsky, G. I. (1983). Instabilities, pattern formation, and turbulence in flames. *Ann. Rev. Fluid Mech.* **15**, 179.

FIGURE CAPTIONS

1. Model geometry; the interface $\bar{x}_3 = \Phi_p(\bar{x}_1, \bar{x}_2, \bar{t})$ denotes the propellant surface.
2. Growth rate ω_1 plotted as a function of the separation distance f_1 for various values of the Lewis number Le , with $N = 100$, $\sigma = .5$ and $\rho_\infty = 1 - \alpha\beta = .5$.
3. Growth rate ω_1 plotted as a function of the separation distance f_1 for various values of the Lewis number Le , with $N = 100$, $\sigma = .5$ and $.3 = \rho_\infty < 1 - \alpha\beta = .5$.
4. Growth rate ω_1 plotted as a function of the separation distance f_1 for various values of the Lewis number Le , with $N = 50$, $\sigma = .5$ and $\rho_\infty = 1 - \alpha\beta = .5$.
5. Growth rate $\omega_1(f_1)$ for $\rho_\infty \lesssim 1 - \alpha\beta \approx 1$, with $N = 40$, $\sigma = .95$ and $Le = .8$.
6. Growth rate $\omega_1(f_1)$ for $\rho_\infty \lesssim 1 - \alpha\beta \approx 1$, with $N = 40$, $\sigma = .95$ and $Le = 1.3$.
7. Growth rate $\omega_1(f_1)$ for $\rho_\infty \lesssim 1 - \alpha\beta \approx .5$, with $N = 40$, $\sigma = .45$ and $Le = .8$.
8. Growth rate $\omega_1(f_1)$ for $\rho_\infty \lesssim 1 - \alpha\beta \approx .5$, with $N = 40$, $\sigma = .45$ and $Le = 1.3$.
9. Growth rate $\omega_1(f_1)$ for $\rho_\infty \lesssim 1 - \alpha\beta \ll 1$, with $N = 40$, $\sigma = .05$ and $Le = .8$.
10. Growth rate $\omega_1(f_1)$ for $\rho_\infty \lesssim 1 - \alpha\beta \ll 1$, with $N = 40$, $\sigma = .05$ and $Le = 1.3$.

propellant surface: $\tilde{x}_3 = \tilde{\Phi}_p(\tilde{x}_1, \tilde{x}_2, \tilde{t})$

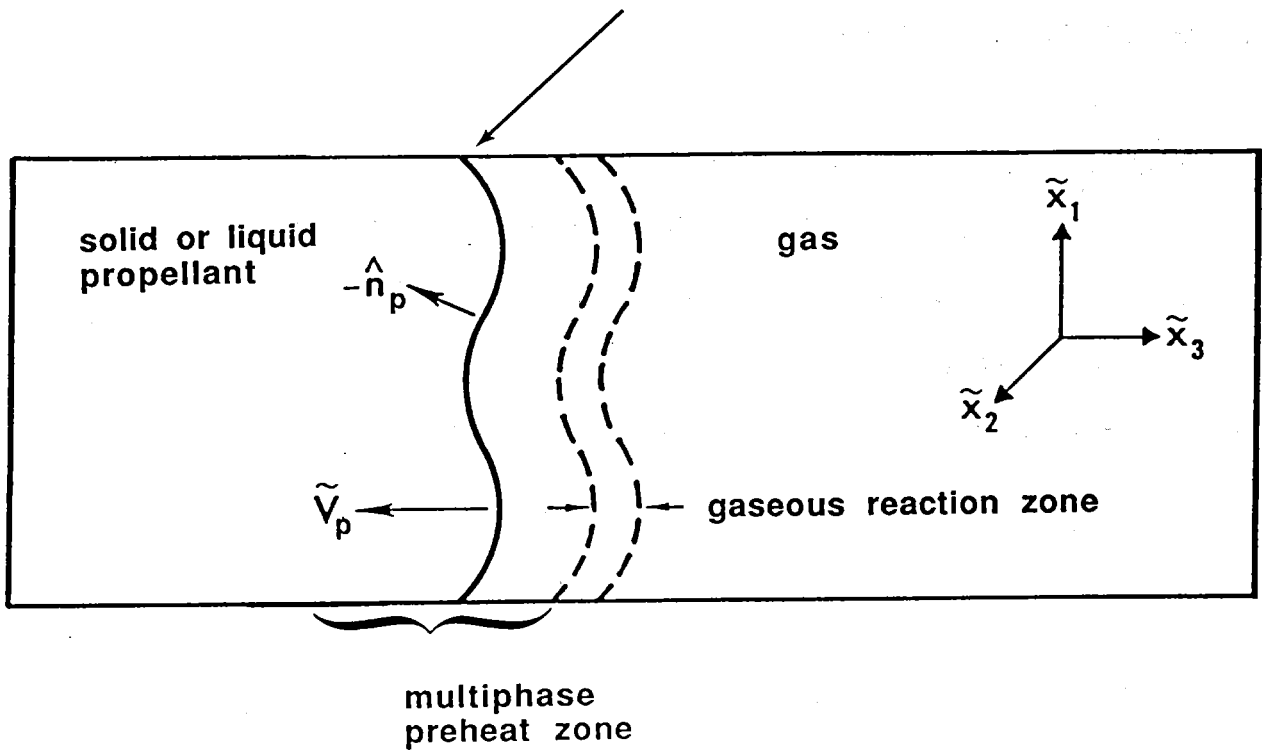


Figure 1

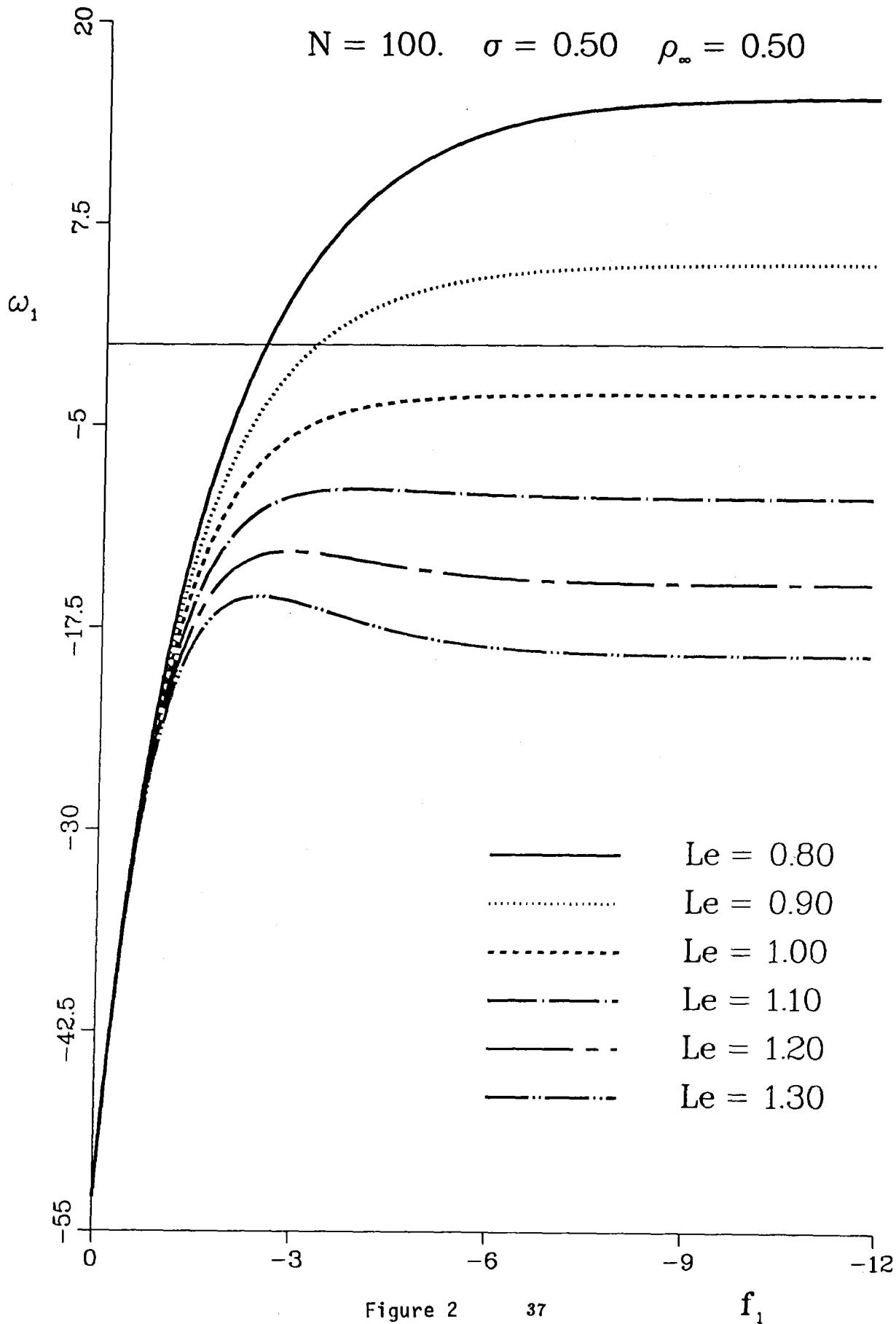


Figure 2

$N = 100. \quad \sigma = 0.50 \quad \rho_{\infty} = 0.30$

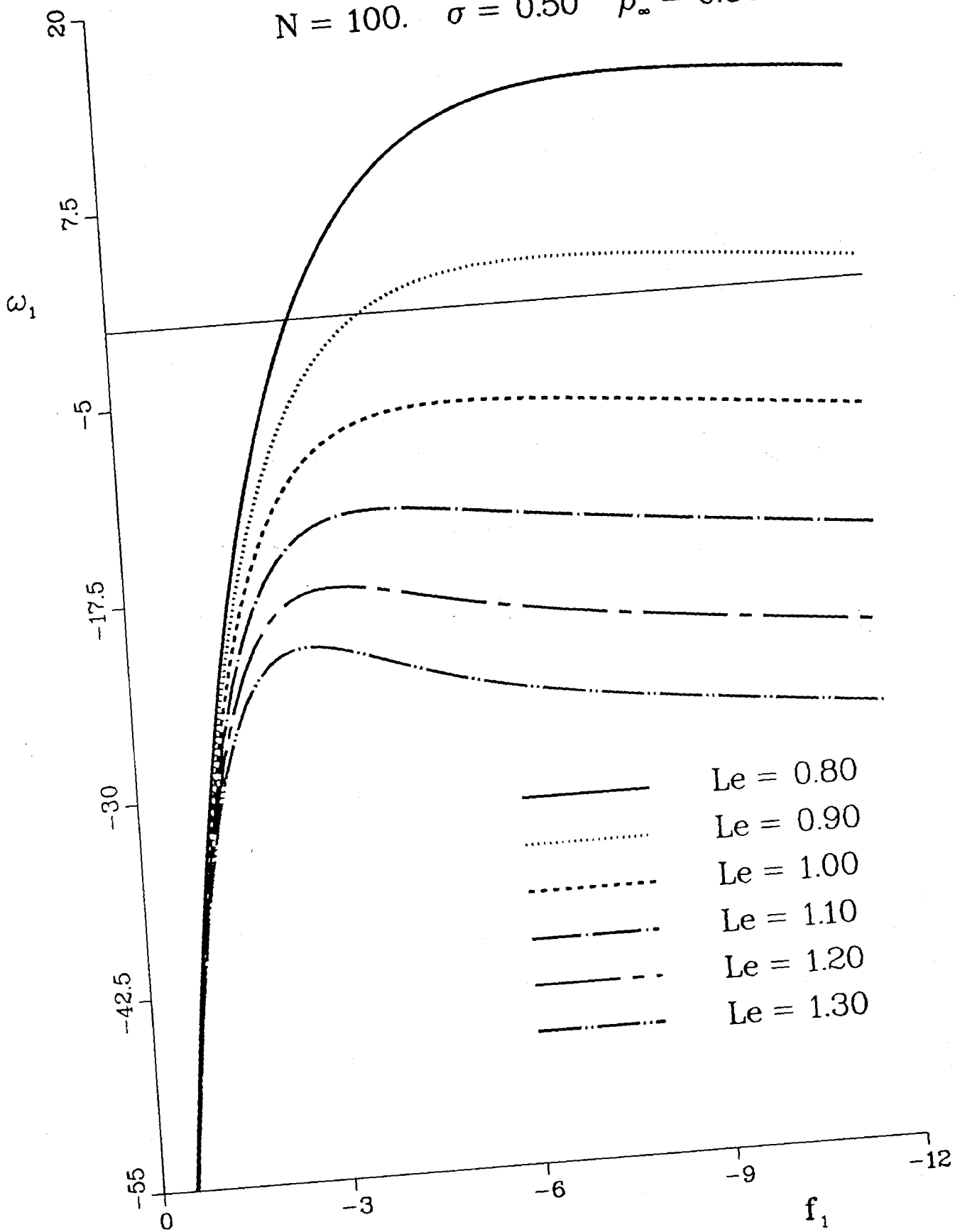


Figure 3 38

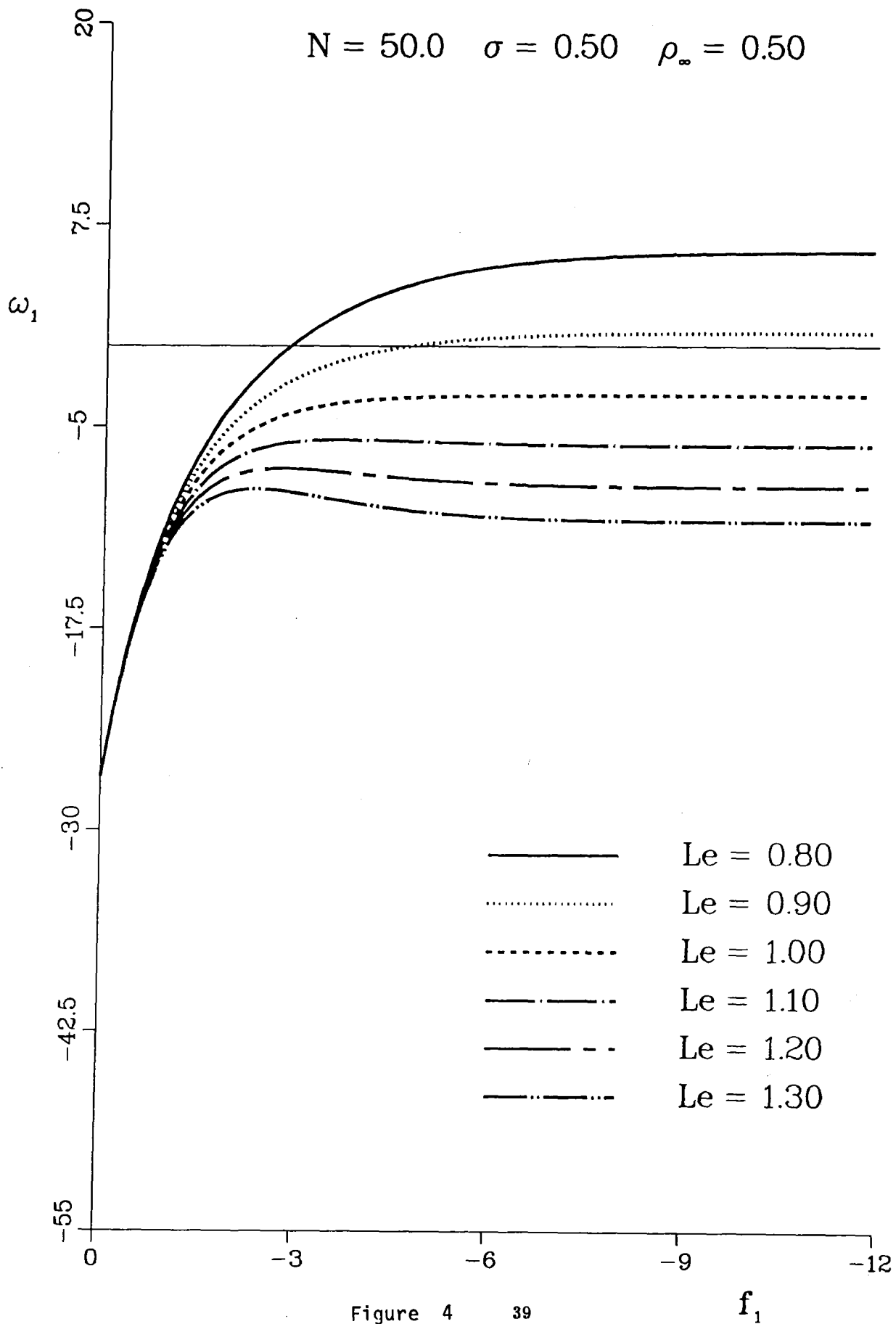


Figure 4 39

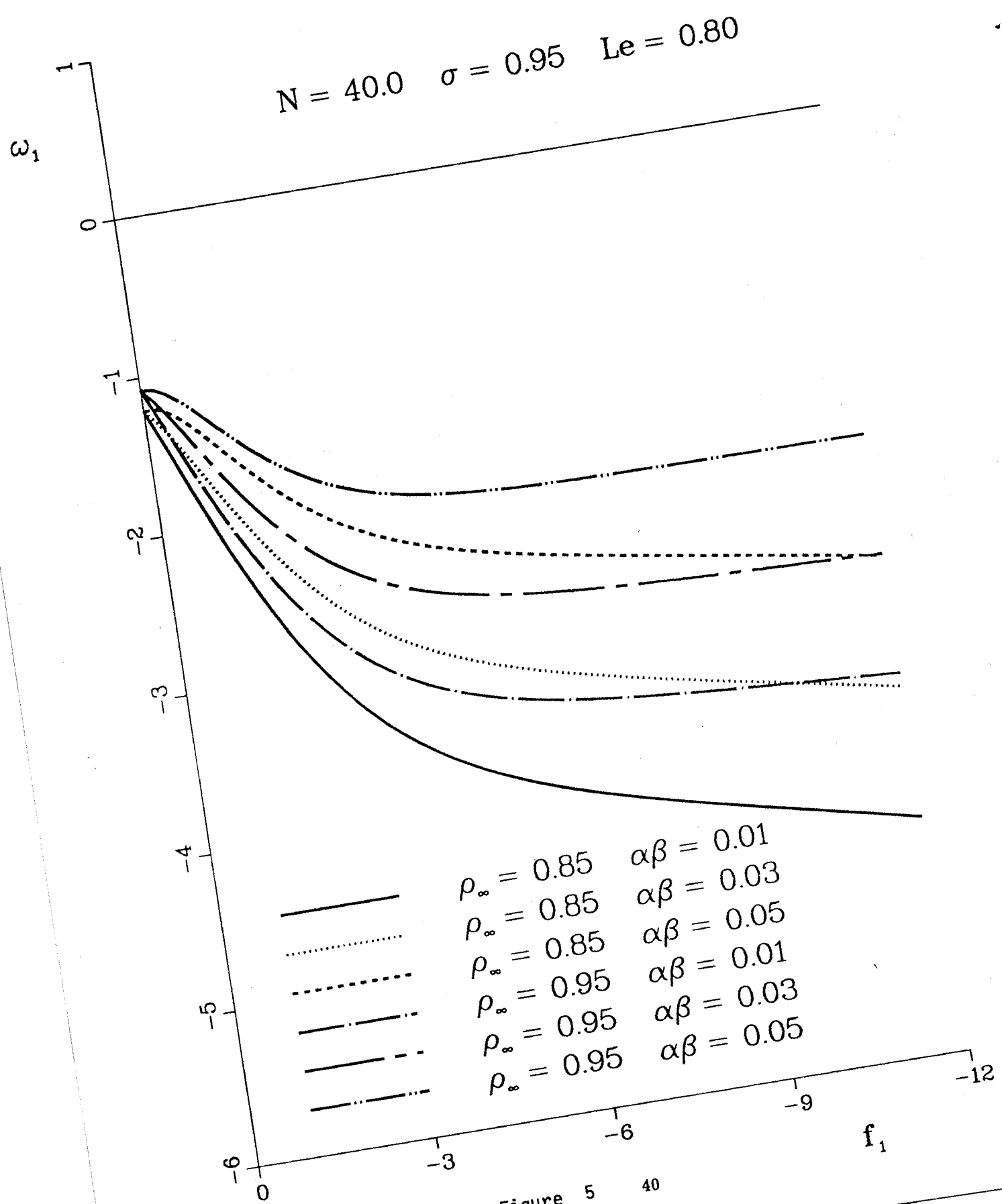


Figure 5 40

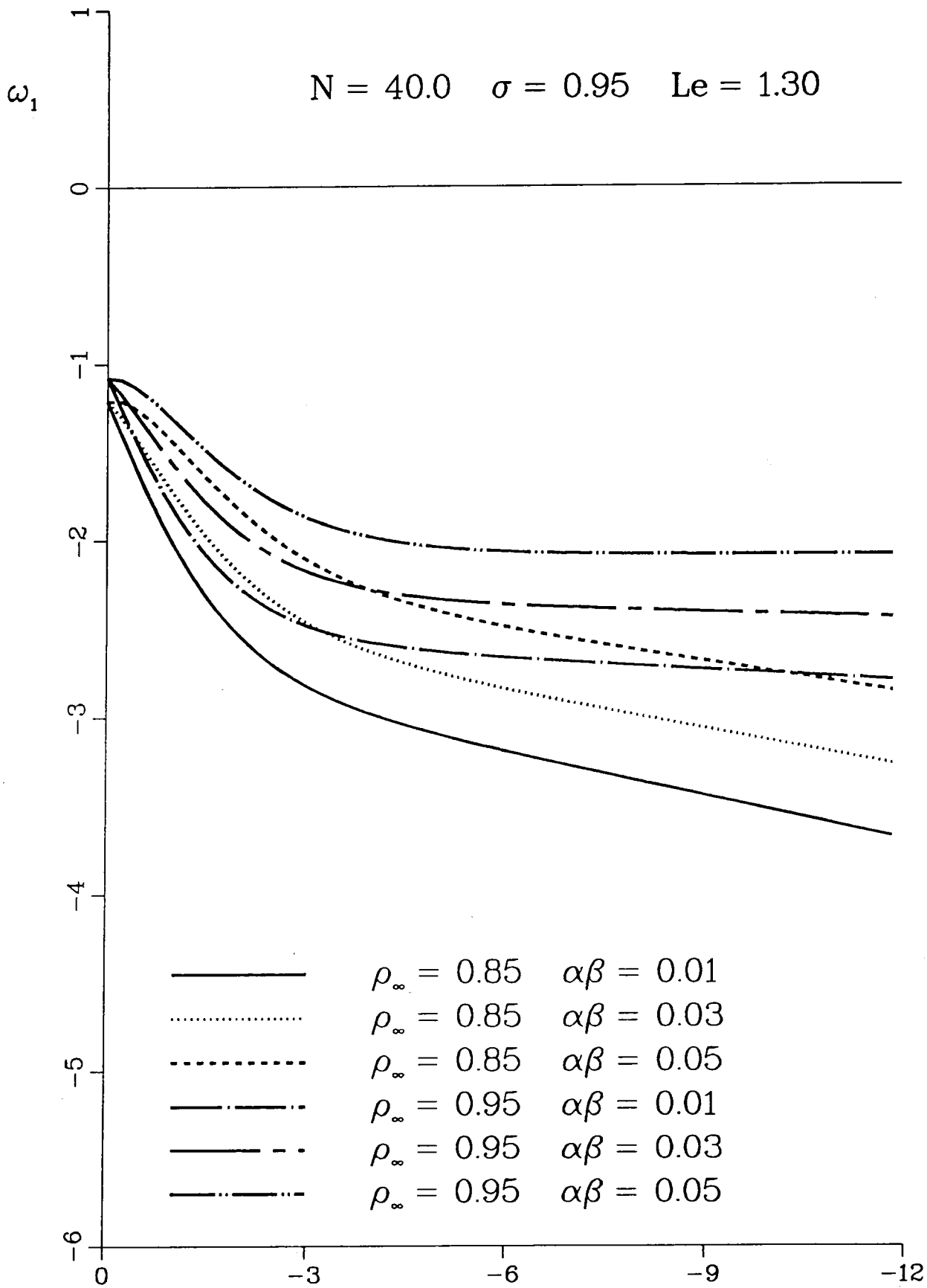


Figure 6

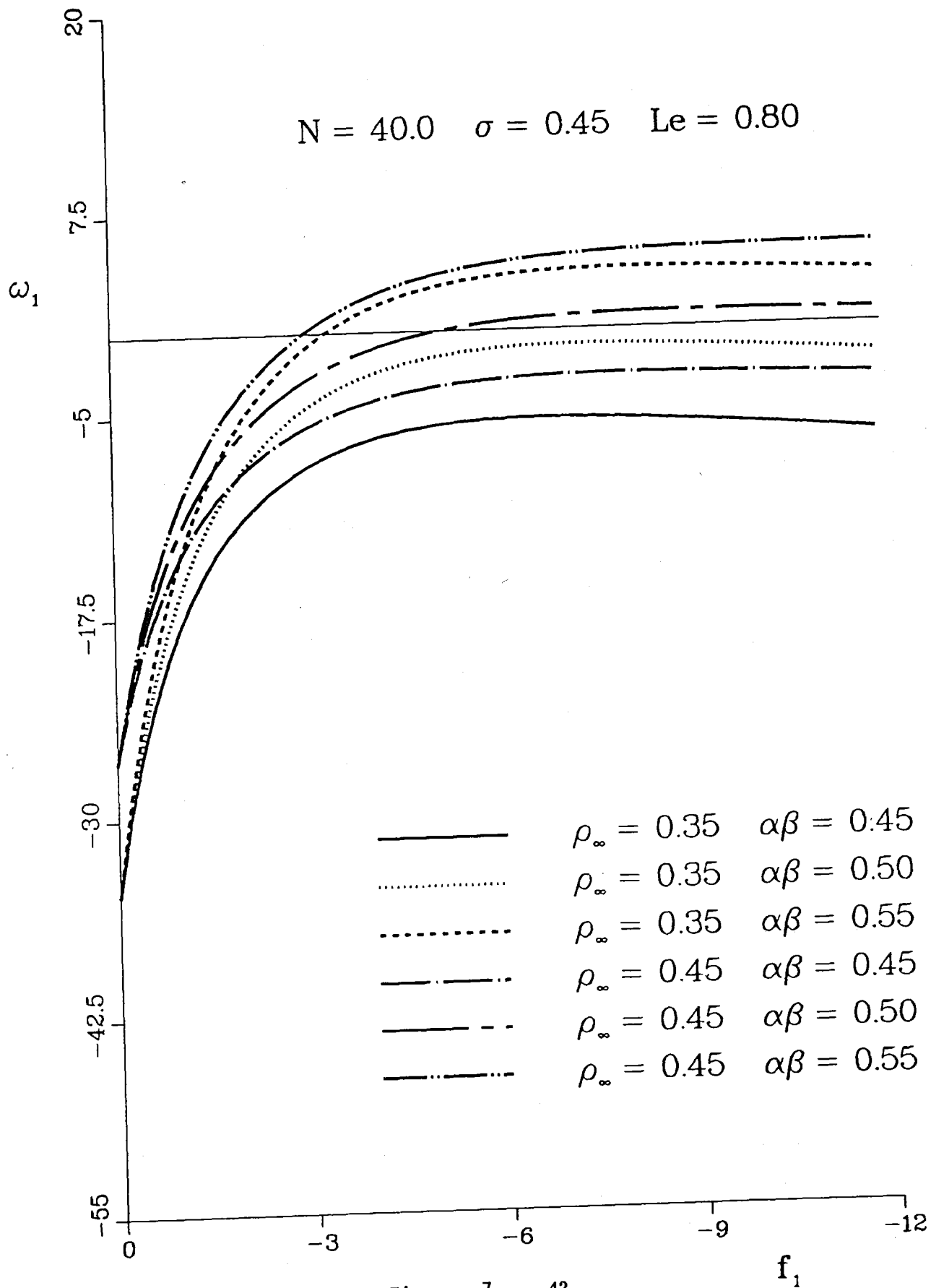


Figure 7 42

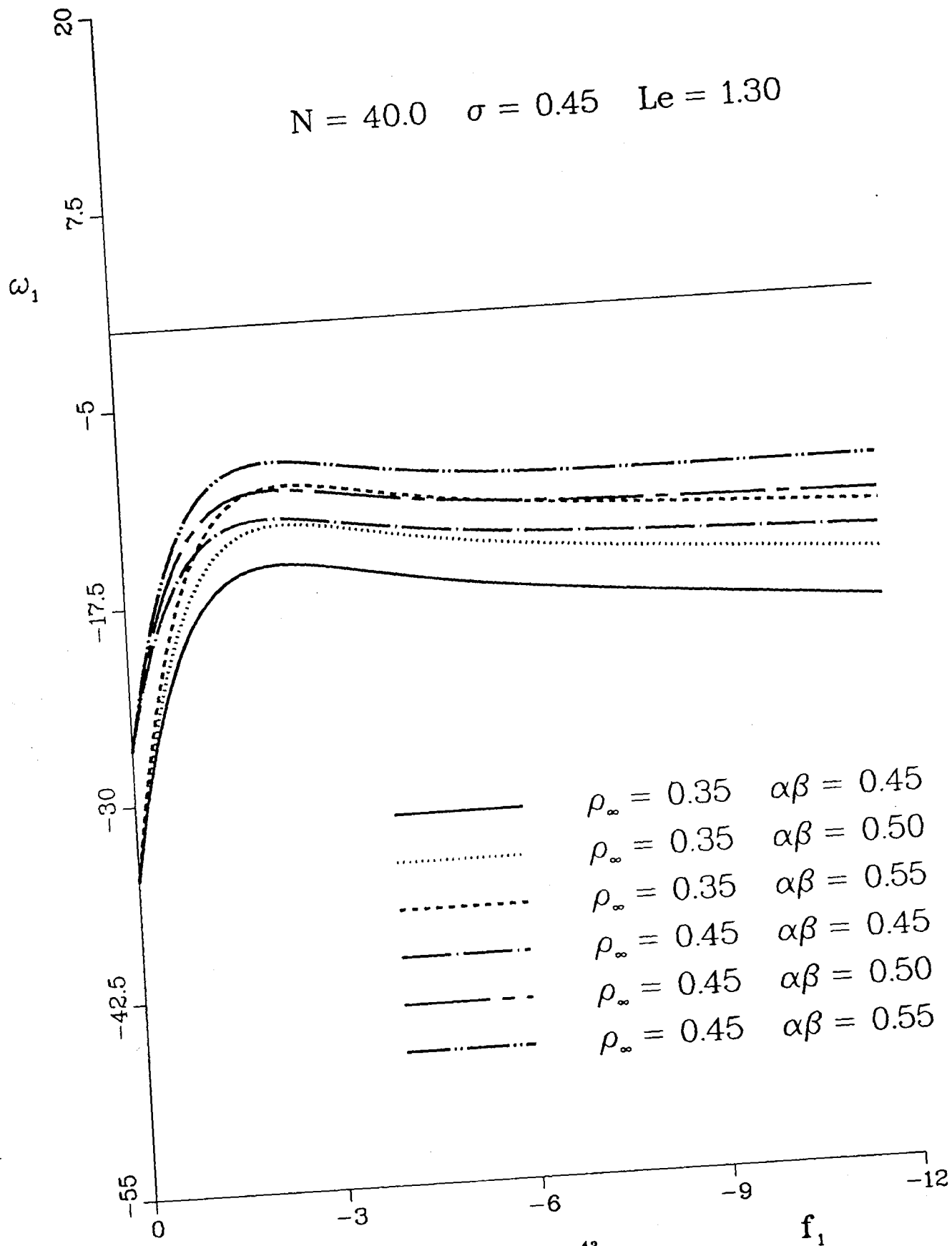


Figure 8

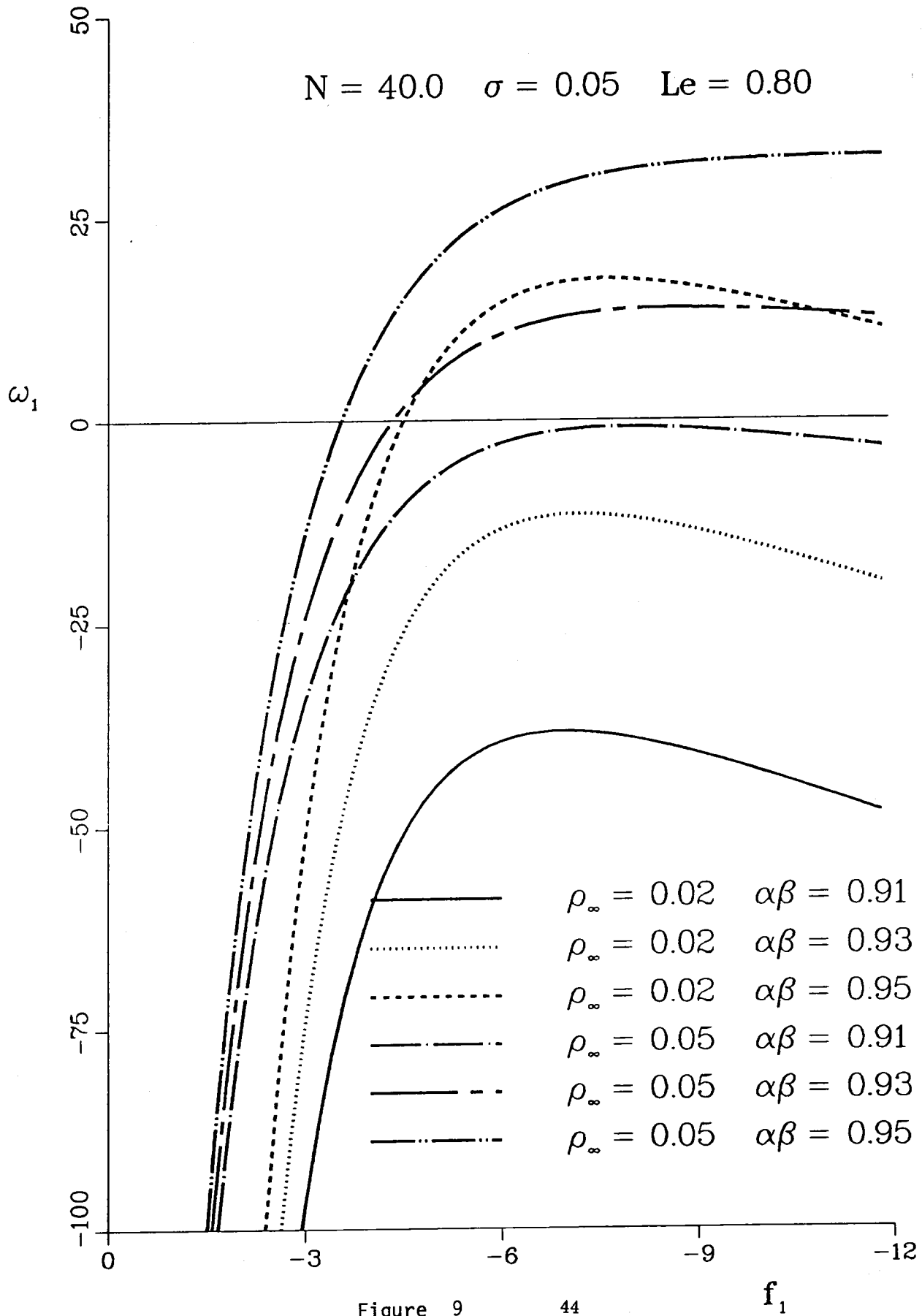


Figure 9

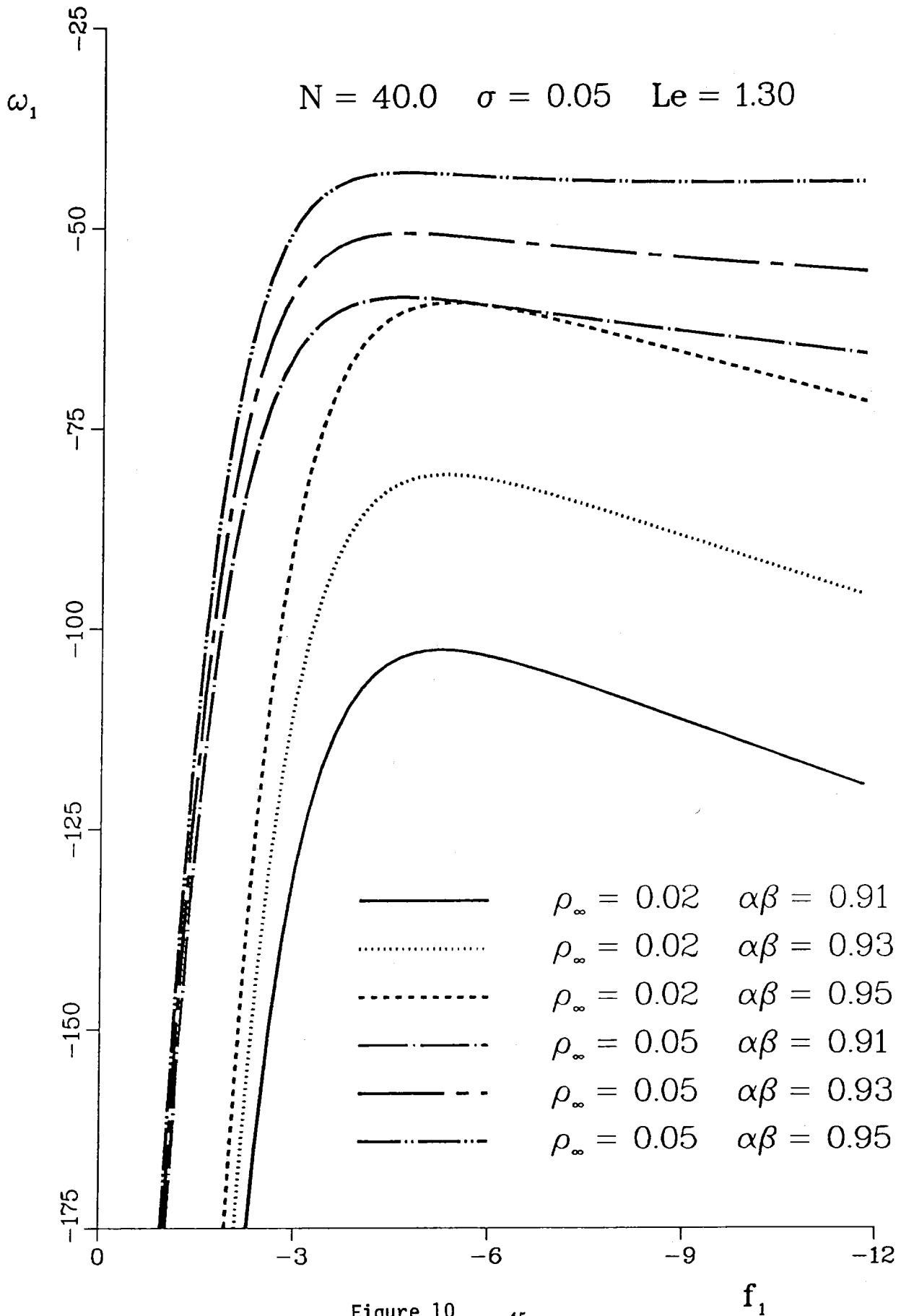


Figure 10

f_1

UNLIMITED RELEASE

INITIAL DISTRIBUTION

Office of Energy Research (6)
U. S. Dept. of Energy
Attn: D. M. Austin
J. Coleman
A. H. Laufer
O. Manley
R. S. Marianelli
F. Dee Stevenson
ER-7, MS G-226 Germantown
Washington DC 20545

Ballistics Research Laboratory (1)
AMXBR-IBD
Attn: G. F. Adams
A. W. Barrows
R. A. Beyer
R. A. Fifer
N. Klein
B. H. Lengsfield
I. W. May
A. W. Miziolek
W. F. Morrison
Aberdeen Proving Ground, MD 21005

Mitat A. Birkan
Program Manager
Directorate of Aerospace Sciences
Dept. of the Air Force
Bolling Air Force Base
DC 20332-6448

Dr. William F. Ballhaus
Director, NASA Ames
Research Center
Moffett Field, CA 94035

Naval Weapons Center (1)
Attn: R. J. Derr
T. Parr
China Lake, CA 93555

U. S. Army Research Office
Attn: R. C. Ghiradelli
D. M. Mann
P. O. Box 12211
Research Triangle Park
North Carolina 27709

Dr. David Weaver, AFRPL
Air Force Rocket Propulsion Lab
DYP/Stop 24
Edwards Air Force Base, CA
93523

Prof. M. Branch
Dept. of Mechanical Engrg.
University of Colorado
Boulder, CO 80309

Prof. T. B. Brill
Dept. of Chemistry
University of Delaware
Newark, DE 19711

Prof. J. F. Clarke
College of Aeronautics
Cranfield Institute of Technology
Cranfield-Bedford MK43 OAL
ENGLAND

Prof. Paul C. Fife
Dept. of Mathematics
University of Arizona
Tucson, AZ 85721

Prof. W. C. Gardiner
Department of Chemistry
University of Texas
Austin, TX 78712

Prof. Martin Golubitsky
Dept of Mathematics
University of Houston
University Park
Houston, TX 77004

Prof. Michael Gorman
Dept. of Physics
University of Houston
Houston, TX 77004

Prof. G. M. Homsy
Dept. of Chemical Engineering
Stanford University
Stanford, CA 94305

F. C. Hoppensteadt, Dean
College of Natural Science
Michigan State University
E. Lansing, MI 48824-1115

Prof. F. A. Howes
Dept. of Mathematics
University of California
Davis, CA 95616

Prof. K. F. Jensen
Chemical Engineering and
Materials Science
151 Amundson Hall
University of Minnesota
Minneapolis, MN 55455

Dr. G. Joulin
Laboratoire D'Energetique
et de Detonique
Universite de Poitiers
Rue Guillaume VII
86034 Poitiers
FRANCE

Prof. D. R. Kasoy
Dept. of Mech. Engrg.
University of Colorado
Boulder, CO 80309

Prof. Barbara Keyfitz
Dept. of Mathematics
University of Houston
University Park
Houston, TX 77004

Prof. K. K. Kuo
Dept. of Mech. Engineering
Pennsylvania State University
University Park, PA 16802

Prof. C. K. Law
Princeton University
Department of Mechanical and
Aerospace Engineering
The Engineering Quadrangle
Princeton University
Princeton, NJ 08544

Prof. Amable Linan
Universidad Politecnica de Madrid
Escuela Tecnica Superior de
Ingenieros Aeronauticos
Plaza del Cardenal Cisneros, 3
Madrid - 3
SPAIN

Prof. J. T. C. Liu
Div. of Engineering, Box D
Brown University
Providence, RI 02912

Prof. J. P. Longwell
Chemical Engineering Dept.
Rm 66554
Massachusetts Inst. of Technology
Cambridge, MA 02139

Prof. Moshe Matalon
Dept. of Engineering Sciences
and Applied Mathematics
Northwestern University
Evanston, IL 60201

Prof. Bernard J. Matkowsky
Dept. of Engineering Sciences
and Applied Mathematics
Northwestern University
Evanston, IL 60201

Prof. A. K. Oppenheim
Dept. of Mechanical Engineering
University of California
Berkeley, CA 94720

Prof. H. B. Palmer
Office of the Dean
Graduate School - 114 Kern Bldg.
Penn State University
University Park, PA 16802

Prof. John Ross
Dept. of Chemistry
Stanford University
Stanford, CA 94305

Prof. Victor Roytburd
Dept. of Mathematical Sciences
Rensselaer Polytechnic Institute
Troy, NY 12128

Prof. M. Sibulkin
Div. of Engineering, Box D
Brown University
Providence, RI 02912

Prof. W. A. Sirignano
Office of the Dean
School of Engineering
University of California, Irvine
Irvine, CA 92717

Prof. L. Sirovich
Div. of Applied Mathematics
Box F
Brown University
Providence, RI 02912

Prof. Mitchell D. Smooke
Dept. of Mechanical Engineering
Yale University
New Haven, CT 06520

Prof. C. H. Su
Div. of Applied Mathematics
Box F
Brown University
Providence, RI 02912

Prof. Cesar Trevino
Departamento de Termica y Fluidos
Universidad Nacional Autonoma de
Mexico
Facultad de Ingenieria
Pacios No. 12, Jardines del Sur
MEXICO 23, D.F.

Prof. Forman A. Williams, UC San Diego
Dept. of Applied Mechanics and
Engineering Science
Univ. of Calif, San Diego
P.O. Box 109
La Jolla, CA 92093

Prof. Vigor Yang
Dept. of Mechanical Engineering
Pennsylvania State University
University Park, PA 16802

Prof. Benn Zinn
Dept. of Aerospace Engineering
Georgia Institute of Technology
225 North Avenue, NW
Atlanta, GA 30332

Seymour B. Alpert
Advanced Power Systems Div.
Electric Power Research Institute
3412 Hillview Avenue
Palo Alto, CA 94308

Prof. Sebastien Candel
Ecole Central des Arts et
Manufactures
Grande Voie de Vignes
92290 Chatenay-Malabry
FRANCE

Prof. Paul Clavin
Laboratoire Dynamique et
Thermophysique des Fluides
Universite de Provence
Centre Saint Jerome
13397 Marseille Cedex 4
FRANCE

Dr. Patrick F. Flynn
Vice President-Research &
Technology
Cummins Engine Company
Mail Code 50181
Box 3005
Columbus, IN 47202-3005

Mr. William R. Gould
Southern California Edison
P. O. Box 800
Rosemead, CA 91770

Dr. Daryl D. Holm
CNLS, MS 457
Los Alamos National Laboratory
P. O. Box 1663
Los Alamos, NM 87545

Dr. Hans Kaper
Applied Mathematics Division
Argonne National Laboratory
9700 S. Cass Avenue
Argonne, IL 60439

Prof. A. K. Kapila
Dept. of Mathematical Sciences
Rensselaer Polytechnic Institute
Troy, NY 12128

Dr. Gary Leaf
Applied Mathematics Division
Argonne National Laboratory
9700 S. Cass Avenue
Argonne, IL 60439

Dr. John Mandzy
General Electric Ordnance
Systems Division
100 Plastics Avenue
Pittsfield, MA 01201

Dr. Basil Nicolaenko
CNLS, MS 457
Los Alamos National Laboratory
P.O. Box 1663
Los Alamos, NM 87545

Prof. R. E. O'Malley
Dept. of Mathematical Sciences
Rensselaer Polytechnic Institute
Troy, NY 12128

Prof. Norbert Peters
Institut für Allgemeine Mechanik
Technische Hochschule Aachen
Aachen
WEST GERMANY

Mr. Eric H. Reichl
P.O. Box 472
Princeton, NJ 08542-0472

Dr. Gerd M. Rosenblatt
Lawrence Berkeley Laboratory
Building 50A, Room 4119
1 Cyclotron Road
Berkeley, CA 94720

R. C. Chin, LLNL, L-321
J. Birch Holt, LLNL, L-369
J. D. Immele, LLNL, L-38
C. K. Westbrook, LLNL, L-321

1420 R. J. Thompson, 1420
Attn: R. C. Allen, 1422

1510 J. W. Nunziato
1513 R. D. Boyd
1530 L. W. Davison
2641 M. R. Scott
2646 L. A. Bertram
6000 D. L. Hartley
8000 J. C. Crawford
Attn: E. E. Ives, 8100
P. E. Brewer, 8500

8200 R. J. Detry
Attn: W. D. Wilson, 8230

8240 C. W. Robinson
Attn: C. M. Hartwig, 8244

8245 R. J. Kee
8300 P. L. Mattern
Attn: R. W. Rohde, 8310
W. Bauer, 8340

8343 M. L. Koszykowski
8350 J. S. Binkley
8351 R. P. Lucht
8353 G. A. Fisk

8354 R. E. Palmer
8357 R. C. Armstrong
8357 R. W. Carling
8357 C. F. Melius
8360 W. J. McLean
8361 D. R. Hardesty
Attn: R. E. Mitchell, 8363

8362 T. M. Dyer
8363 J. K. Bechtold (30)
8363 S. B. Margolis (30)
8363 B. R. Sanders
Attn: W. T. Ashurst, 8363
P. K. Barr, 8363
H. A. Dwyer, 8363
A. R. Kerstein, 8363
K. D. Marx, 8363

8364 S. C. Johnston
8400 R. C. Wayne
8442 R. E. Stoltz
8470 R. L. Rinne
8535 Publication Division,
Tech. Lib. Proc. Div., 3141
3141 Technical Library Processes
Division, (3)
8524 Central Technical
Files (3)



8232-2/068625



00000002 -



8232-2/068625



00000002 -



8232-2/068625



00000002 -
